RESEARCH ARTICLE

International Journal of Climatology | RMetS

High-resolution dynamically downscaled rainfall and temperature projections for ecological life zones within Puerto Rico and for the U.S. Virgin Islands

Jared H. Bowden[1] | Adam J. Terando[1,2] | Vasu Misra[3,4,5] |
Adrienne Wootten[6] | Amit Bhardwaj[4,5] | Ryan Boyles[1,2] | William Gould[7] |
Jaime A. Collazo[1,8] | Tanya L. Spero[9]

[1]Department of Applied Ecology, North Carolina State University, Raleigh, North Carolina

[2]Southeast Climate Adaptation Science Center, Raleigh, US Geological Survey, North Carolina

[3]Department of Earth, Ocean, and Atmospheric Science, Florida State University, Tallahassee, Florida

[4]Center for Ocean-Atmospheric Prediction Studies, Florida State University, Tallahassee, Florida

[5]Florida Climate Institute, Florida State University, Tallahassee, Florida

[6]South Central Climate Adaptation Science Center, Norman, Oklahoma

[7]International Institute of Tropical Forestry, San Juan, Puerto Rico

[8]US Geological Survey, North Carolina Cooperative Fish and Wildlife Research Unit, Raleigh, North Carolina

[9]Office of Research and Development, U. S. Environmental Protection Agency, Research Triangle Park, Triangle Park, NorthCarolina

Correspondence

Jared H. Bowden, North Carolina State University, 100 Eugene Brooks Avenue, Campus Box 7617, Raleigh, NC 27695-7617.
Email: jhbowden@ncsu.edu

Abstract

The weather research and forecasting (WRF) model and a combination of the regional spectral model (RSM) and the Japanese Meteorological Agency Non-Hydrostatic Model (NHM) were used to dynamically downscale selected CMIP5 global climate models to provide 2-km projections with hourly model output for Puerto Rico and the U.S. Virgin Islands. Two 20-year time slices were downscaled for historical (1986–2005) and future (2041–2060) periods following RCP8.5. Projected changes to mean and extreme temperature and precipitation were quantified for Holdridge life zones within Puerto Rico and for the U.S. Virgin Islands. The evaluation reveals a persistent cold bias for all islands in the U.S. Caribbean, a dry bias across Puerto Rico, and a wet bias on the windward side of mountains within the U.S. Virgin Islands. Despite these biases, model simulations show a robust drying pattern for all islands that is generally larger for Puerto Rico (25% annual rainfall reduction for some life zones) than the U.S. Virgin Islands (12% island average). The largest precipitation reductions are found during the more convectively active afternoon and evening hours. Within Puerto Rico, the model uncertainty increases for the wetter life zones, especially for precipitation. Across the life zones, both models project unprecedented maximum and minimum temperatures that may exceed 200 days annually above the historical baseline with only small changes to the frequency of extreme rainfall. By contrast, in the U.S. Virgin Islands, there is no consensus on the location of the largest drying relative to the windward and leeward side of the islands. However, the models project the largest increases in maximum temperature on the southern side of St. Croix and in higher elevations of St. Thomas and St. John.

KEYWORDS

climate change, Puerto Rico, regional climate modelling, USVI

1 | INTRODUCTION

Islands in the northern Caribbean are vulnerable to extreme weather-related disasters. The projected increase in global greenhouse gases (GHGs) depicts a world with an increasing threat of widespread drought (Dai, 2013) and stronger tropical cyclones with higher rainfall rates (Knutson et al., 2019a; 2019b). Recently, in 2015, Puerto Rico, located in the northern Caribbean, experienced one of the most severe droughts within the island's observational record in 2015 (Álvarez-Berríos et al., 2018) and just 2 years later took a direct hit from Hurricane Maria in which rainfall totals exceeded 30 in. within some parts of the island (Pasch et al., 2019). Hurricane Maria is one of the deadliest and costliest storms in U.S. history with an estimated 3,000 deaths (Santos-Burgoa et al., 2018) and costs exceeding 90 billion USD (NOAA NCEI, 2019).

These recent disasters are concerning, especially when they are put into the context of observed and simulated changes within the climate system. Puerto Rico and neighbouring islands lie at the edge of the convective zone of the tropics but are projected to experience significant reductions in total precipitation (i.e., "drying") this century as GHGs and temperatures increase (Neelin et al., 2006). Lau and Kim (2015) discuss projected changes in precipitation at the subtropical margins from an ensemble of global climate models. The study illustrates a future climate with more intense tropical convection organized over a narrower region which in return favours a drier subtropical atmosphere, especially on the equatorward side of the subtropical margins as a result of enhanced subsidence. This large-scale "subtropical" precipitation decline is considered part of the "dry get drier" and "upped-ante" phenomenon first proposed by Held and Soden (2006). He and Soden (2017) caveated the finding of declining subtropical precipitation by noting that the drying pattern is primarily limited to over the ocean. He and Soden (2017) illustrate that this precipitation decline is a response to the continental land-sea warming contrast, the direct radiative forcing of CO_2, and sea surface temperature pattern changes within the northwest Atlantic and southeast Pacific. Dai et al. (2018) further show the reduction in subtropical precipitation is likely to be a persistent feature in a warmer climate and not just a transient response to an increase in GHGs. However, studying future drought events associated with large-scale changes in the atmosphere becomes complicated for many subtropical islands when also considering extreme rainfall from tropical cyclones. Warming sea surface temperatures have been correlated with weaker wind shear within the Caribbean (Kossin and Vimont, 2007; Vimont and Kossin, 2007; Kossin, 2017),

so the atmosphere is more conducive to producing stronger storms. Additionally, tropical cyclones may intensify more quickly as the oceans continue to warm (Emanuel, 2017) and move more slowly (Kossin, 2018), as observed with Hurricanes Harvey (2017), Florence (2018), and Dorian (2019). Despite the possibility of stronger and slower-moving tropical cyclones with intense rainfall, the Caribbean warrants more attention as the exposure to long-term drying becomes more likely as a result of large-scale changes in the atmospheric circulation. These changes within the atmosphere will likely create additional stresses to vulnerable ecosystems, water resources, and human well-being.

Numerous studies have attempted to quantify the projected changes to rainfall and temperature within the Caribbean as GHGs increase, including analysing output from coupled global climate models (Karmalkar et al., 2013; Taylor and Clarke, 2018), high resolution time-slice global atmospheric models (Hall et al., 2013), dynamical downscaling (Campbell et al., 2011; Bhardwaj et al., 2018), and statistical downscaling (Hayhoe, 2013; Henareh et al., 2016). Generally, these studies focused on quantifying rainfall and temperature changes for large regions that grouped multiple small island states that exhibit similar annual cycles and inter-annual variability (e.g., Campbell et al., 2011; Hall et al., 2013; Karmalkar et al., 2013; Taylor and Clarke, 2018). These studies add value by highlighting the projected regional and seasonal changes for areas within the Caribbean. Karmalkar et al. (2013) reviewed the projected changes from phase 3 of the Climate Model Intercomparison Project (CMIP3) and regional climate modelling from UK Hadley Centre modelling system in PRECIS (Providing Regional Climates for Impact Studies). Karmalkar et al. (2013) found more drying for the latter half of the 21st century with the strongest drying occurring during the early part of the wet season and within the western half of Caribbean. However, the magnitude of the drying was less certain, especially when including output from higher resolution regional climate models that better resolve the small island states. Using the more recent global climate model output from phase 5 of the Climate Model Intercomparison Project (CMIP5), Taylor and Clarke (2018) analysed the Caribbean's future climate when mean global surface air temperatures are 1.5°C, 2.0°C, and 2.5°C above pre-industrial values (1861–1899). They showed that there is a shift to predominately drier conditions throughout Caribbean and an extension of warm spells of up to 70 days that occurs between 1.5°C and 2.0°C mean global warming.

One shortcoming of many prior modelling studies is the inability to resolve the terrain that interacts with the

prevailing trade winds. This interaction is extremely important because it helps create the large precipitation and temperature gradients within the islands over short distances (<10 km). The sharp precipitation gradients promote a rich mosaic of habitats. Puerto Rico and the U.S. Virgin Islands are ideal locations to perform high-resolution dynamical downscaling because these islands have large precipitation gradients that primarily result from moist easterly trade winds impinging upon the island mountains. Puerto Rico's climate includes stark contrasts—such as the El Yunque rainforest located on the northeast side within the Sierra de Luquillo mountain range and the Guanica dry forest south of the Cordillera Central mountain range—less than 100 km from each other and requires finer-resolution modelling to capture, Figure 1. These sharp contrasts are important to the distribution of Holdridge ecological life zones defined using the mean annual biotemperature, mean annual precipitation, and annual potential evapotranspiration ratio (Ewel and Whitmore, 1973). Additionally, high-resolution modelling is needed to simulate the interaction between the easterly trade winds with the Cordillera Central mountain range which supports organized afternoon convection on the western side of the island (Jury and Chiao, 2013). The need for higher-resolution climate change projections is further supported by recent precipitation trends across Puerto Rico that vary with elevation (Van Beusekom *et al.*, 2016).
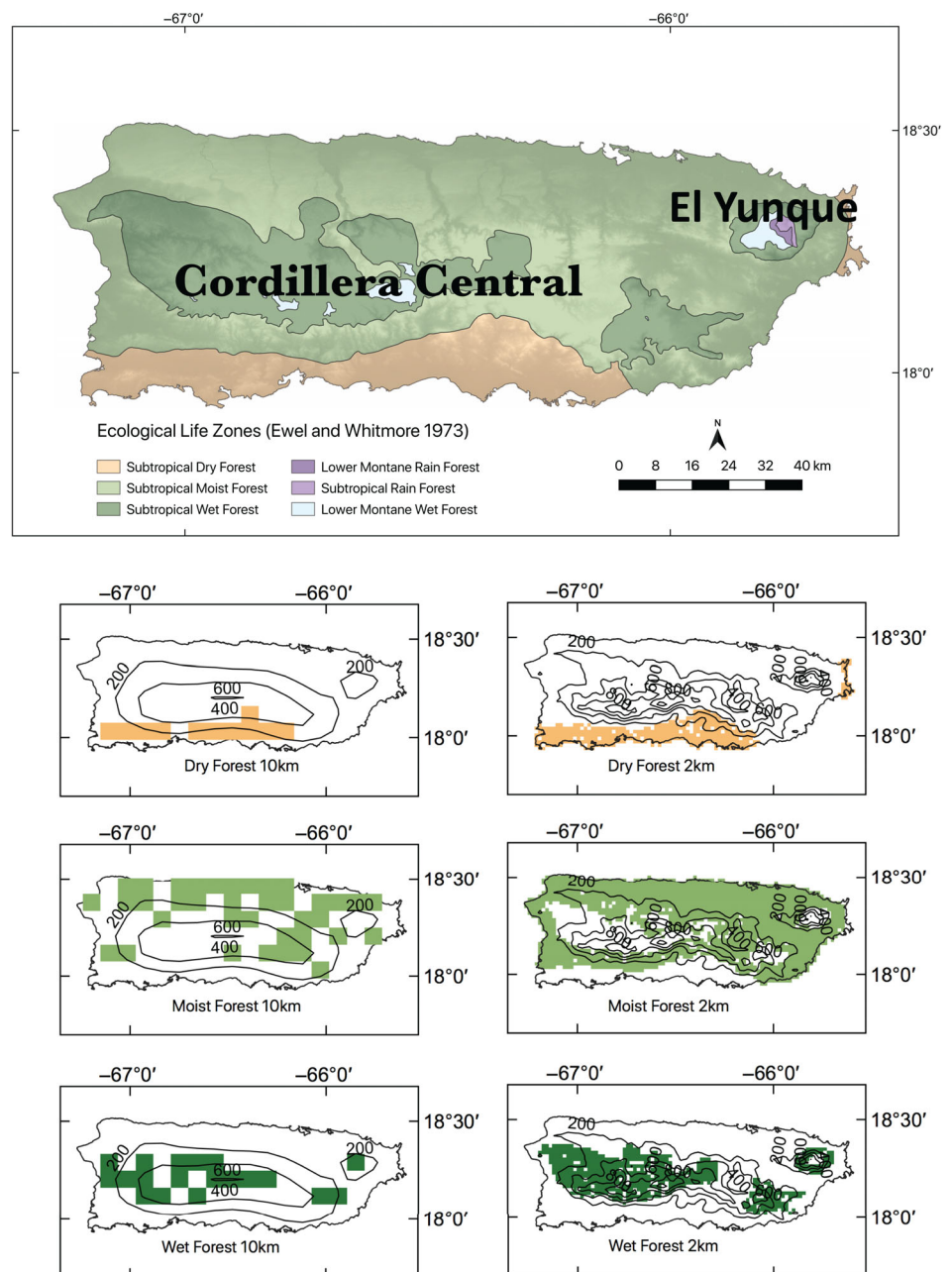

FIGURE 1 Observed ecological life zones within Puerto Rico (top) and model representation for the 10-km (left) and 2-km (right) WRF domains with model terrain height (contoured in meters)

Simulating an elevation-dependent climate response within complex topography requires horizontal grid spacing of 5-km or less (Rasmussen *et al.*, 2011). Recently, Bhardwaj *et al.* (2018) used a non-hydrostatic regional climate model at 2-km horizontal grid spacing to investigate climate change within Puerto Rico at mid-twenty-first century following Representative Concentration Pathway 8.5 (RCP8.5). Their study found a diminished mid-summer drought, which is a temporary dry period during the rainy season, in the northwestern portion of the island and less frequent extreme rainfall at sub-daily and daily time scales. The frequency of occurrence of the most extreme rainfall in this dynamically downscaled realization contradicts statistically downscaled projections within Puerto Rico which show an increase in number of days for most extreme precipitation (Hayhoe, 2013). Furthermore, Henareh *et al.* (2016) use the statistical downscaling of Hayhoe (2013) to map the possible ecological effects of climate change for the Holdridge life zones and finds a shift to drier life zones with the possibility of losing the subtropical rain forests within Puerto Rico by the end of the century. The statistical downscaling consensus was drawn from a large ensemble of GCMs and scenarios, suggesting that the dynamical downscaled realization from Bhardwaj *et al.* (2018) could be sensitive to the GCM, the scenario, and regional climate model and its configuration. Another possibility is the statistically downscaled projections may not accurately represent the complex climate, especially with regards to changing precipitation extremes as both the stationarity assumption and station density are known issues with statistical downscaling.

This study is an extension of the Bhardwaj *et al.* (2018) study and includes additional dynamically downscaled high-resolution (2-km) climate change realizations for RCP8.5, with an overall climate forcing of 8.5 W m^{-2} by the end of the 21st century (Riahi *et al.*, 2011). These simulations downscale multiple GCMs centered on the mid-21st century using two different regional climate modelling systems to explore whether additional dynamically downscaled models would corroborate Bhardwaj et al. This manuscript also complements Henareh *et al.* (2016), as we also investigate climate change within the Holdridge ecological life zones. In this study, high-resolution dynamically downscaled simulations are evaluated against observations to quantify the model errors and projected temperature and precipitation changes for the three largest Holdridge life zones within Puerto Rico, resolved by the RCMs as shown in Figure 1, and for the U.S. Virgin Islands. This analysis includes quantifying changes to the mean and extremes within these life zones in Puerto Rico, including the diurnal cycle and tails of the distributions where large uncertainties and little

information exist regarding climate change. To our knowledge this is the first study that provides regional climate change information for the U.S. Virgin Islands. In the conclusions, we highlight key points important for stakeholders considering regional climate change projections for the U.S. Caribbean islands including uncertainties, modelling challenges, and suggestions to improve regional climate change projections for the islands.

2 | MODEL EXPERIMENTS AND EVALUATION

This study uses two regional climate modelling systems to downscale select global climate models that participated in CMIP5. Each regional climate model applied a unique model configuration to generate projections for Puerto Rico and the U.S. Virgin Islands at 2-km horizontal grid spacing. Each regional climate model downscaled two 20-year time slices from two CMIP5 global climate models (Taylor *et al.*, 2012): a historical time slice (1986–2005) and a future time slice (2041–2060) for RCP8.5. Each regional climate model downscaled the same CMIP5 model for comparison. The future time period, GHG emission scenario, and model output parameters archived were selected based on workshop recommendations from stakeholders within Puerto Rico and the U.S. Virgin Islands, including ecologists, biologists, and hydrologists. Included in Table 1 is a

TABLE 1 Mean annual 2-m temperature and precipitation change from CMIP5 GCMs for mid-century (2041-2060 minus 1986-2005) for RCP8.5 averaged over the U.S. Caribbean

GCM	T2 Mean (°C)	Precipitation (% change)
CCSM4	+1.3	−23
CNRM-CM5	+1.0	−2
GFDL-ESM2G	+1.1	−5
ACCESS1-3	+1.9	−19
CSIRO-Mk-3-6-0	+1.5	−10
FGOALS-G2	+1.3	−2
GISS-E2-R	+1.2	−3
HadGEM2-CC	+1.6	−31
IPSL-CM5A-LR	+1.8	−1
MPI-ESM-MR	+1.6	−22
NorESM-M	+1.1	−18

Note: Only the first realization from each GCM is shown. The U.S. Caribbean defined by the high-resolution nest in the top panel of Figure 2. CMIP5 GCMs in bold are dynamically downscaled over the U.S. Caribbean.

comparison of the projected temperature and precipitation changes averaged over the U.S. Caribbean for the three CMIP5 GCMs downscaled, discussed more below, as well as eight additional CMIP5 GCMs for the same 20-year time slices. Table 1 is included to provide additional context given known problems when identifying regional climate change signals, such as the benefit of sampling internal "unforced" climate variability with large ensembles, as in Deser *et al.* (2012), as well as potential problems when downscaling a subset of GCMs, as in Mezghani *et al.* (2019).

2.1 | Weather research and forecasting model

One regional climate model used in this study is the weather research and forecasting (WRF) model version 3.6.1 (Skamarock and Klemp, 2008). The WRF model was used to dynamically downscale two CMIP5 models: the Community Climate System Model (CCSM4; Gent *et al.*, 2011) and the Centre National de Recherches Meteorologiques-CERFACS (CNRM; Voldoire *et al.*, 2013). WRF was configured to use a 30–10-2-km simultaneous one-way nest (Figure 2). It is
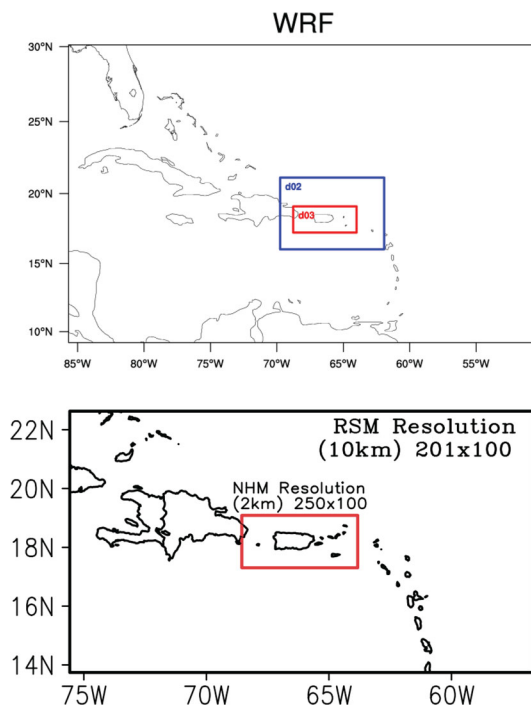

FIGURE 2 WRF (top) and RSM-NHM (bottom) domains. WRF applies a one-way nest with a 30km-10km-2-km domain. RSM simulations (10-km) are used as lateral boundary conditions to the NHM (2-km)

important to note that CMIP5 models have lower errors than the prior generation of global climate models, including the annual temperature cycle of the Caribbean (Ryu and Hayhoe, 2014). In particular, the CNRM 20th-century simulations improve the fidelity of the annual temperature cycle compared to other CMIP5 models (see figure 5 of Ryu and Hayhoe, 2014) and simulate the seasonal precipitation cycle that realistically reflects both a mid-summer drought and two precipitation peaks within the Caribbean (see table 3 of Hayhoe, 2013). Table 1 includes temperature and precipitation changes for 11 CMIP5 GCMs. For CNRM, the mean warming for the U.S. Caribbean is 1°C with small to insignificant drying of −2%. In comparison, CCSM4 improves the simulation of oceanic features that affect the natural variability in the Caribbean, such as El Niño Southern Oscillation (ENSO; Bellenger *et al.*, 2014) with significant rainfall reduction, −23%, for RCP8.5 by mid-century with a mean warming of 1.3°C. Finally, the best performing WRF configuration identified in Wootten *et al.* (2016) was used in this study. Some important WRF model options include applying analysis nudging within the outer two domains and using a convective parameterization scheme for the innermost domain to reduce rainfall bias, as discussed in detail within Wootten *et al.* (2016). The following physics options were selected for the WRF simulations:

- Radiation—RRTMG (Iacono *et al.*, 2008)
- Microphysics—WSM6 (Hong and Lim, 2006)
- Planetary Boundary Layer—YSU (Hong *et al.*, 2006)
- Land Surface—Noah (Chen and Dudhia, 2001)
- Convection—Modified Kain Fritsch (Herwehe *et al.*, 2014)

2.2 | Regional spectral model and Japanese meteorological agency non-hydrostatic model

The second configuration used two different regional climate models, the hydrostatic regional spectral model (RSM; Kanamitsu *et al.*, 2010) and the non-hydrostatic model (NHM; Saito *et al.*, 2006). The RSM downscaled the global climate models to a 10-km horizontal grid spacing (Figure 1). RSM uses a scale-selective bias correction (Misra, 2007), which serves to maintain large-scale consistency within the regional climate model with scales resolved within the driving global climate model in a manner similar to analysis nudging in WRF (Bowden *et al.*, 2012; Otte *et al.*, 2012; Bowden *et al.*, 2013).

The RSM was also used to downscale CCSM4 (for comparison with WRF), as well as the Geophysical Fluid Dynamics Laboratory Coupled Physical Model (GFDL-ESM2G; Dunne *et al.*, 2012). Hayhoe (2013) noted that GFDL-ESM2G erroneously simulated just one precipitation peak for the U.S. Caribbean—a feature more commonly observed in the eastern Caribbean—and this deficiency adversely affects the downscaled simulations. Projected changes for the GFDL-ESM2G is closer to that of CNRM with 1.1°C warming and small rainfall reduction of −5%. The output from hydrostatic RSM was used as lateral boundary conditions to the NHM to further downscale CCSM4 and GFDL-ESM2Gto 2-km. Unlike WRF, the NHM does not offer a convective parameterization scheme, so the comparisons of precipitation are another a unique aspect of this study. Below is a list of the RSM and NHM physics.

RSM Physics:

- Radiation—shortwave (Chou and Lee, 1996); longwave (Chou and Suarez, 1994)
- Microphysics—based on Slingo (1987)
- Planetary Boundary Layer—following Hong and Pan (1996)
- Land Surface—following Ek *et al.* (2003)
- Convection—shallow (Tiedtke *et al.*, 1988); deep (Pan and Wu, 1995)

NHM Physics:

- Radiation—based on Sugi *et al.* (1990)
- Microphysics—explicit three ice bulk scheme (Ikawa and Saito, 1991)
- Planetary Boundary Layer—Mellor-Yamada level 3 (Nakanishi and Niino, 2006)
- Land Surface—parameterization following Beljaars and Holtslag (1991)

2.3 | Model evaluation

For both Puerto Rico and the U.S. Virgin Islands, we only focus on the model output from the 2-km simulations. Specifically, each simulation is evaluated within Puerto Rico for three of the six Holdridge life zones: subtropical dry forest, subtropical moist forest, and subtropical wet forest. We do not perform an analysis for the other life zones within Puerto Rico because the 2-km resolution does not sufficiently resolve these life zones, including lower montane wet forest, lower montane rainforest, and subtropical rain forest. Figure 1 illustrates how the life zones and the ground elevation are represented in WRF at 10-km and at 2-km within Puerto Rico. The 10-km

domain cannot resolve important terrain features within the Sierra de Luquillo and Cordillera Central mountain ranges, so the model does not sufficiently resolve the observed ecologically relevant life zones, especially the subtropical dry and wet forests that provide unique habitats. For example, the subtropical dry forest along the southern coast is underrepresented at 10-km compared with 2-km.

The historical monthly maximum and minimum temperature and monthly accumulated precipitation for the subtropical dry/moist/wet forests within Puerto Rico are evaluated against the monthly climatology from the Parameter-Elevation Regressions on Independent Slopes Model (∼4-km PRISM; Daly *et al.*, 2003) to quantify the average model bias for each life zone within Puerto Rico. The PRISM data for Puerto Rico is available only as a climatological normal calculated for the period 1963–1995. One significant advantage of PRISM for this study is the ability to evaluate elevation relationships that are critical to the microclimates within the island, especially the different life zones. We then quantify and discuss uncertainty in the downscaled projections for both temperature and precipitation, including changes to the diurnal cycle and extremes, for each of the life zones, which is particularly important for natural, cultural, and water resource managers (e.g., species conservation). The significance of the projected changes is calculated using a two-sided non-parametric Mann–Whitney U-test (Wilks, 2006) at the 95% confidence level. This test does not assume the distribution is normal, and uses ranks to assess if the data, simulated temperature or precipitation, is significantly shifted higher or lower in the future period.

Unlike Puerto Rico, gridded rainfall and temperature products like PRISM are unavailable for evaluation within the U.S. Virgin Islands: St. John, St. Thomas, and St. Croix. Here we use station climatological normals (U.S. Climate Normals Data from 1981–2010; Arguez *et al.*, 2012) to evaluate the 2-km downscaled mean temperature and accumulated precipitation. We then quantify the island average projected changes to annual average maximum and minimum temperature and accumulated rainfall. In addition, projected temperature and precipitation changes for each island are shown to highlight areas with large differences as well as areas with similarities.

3 | RESULTS

3.1 | Puerto Rico—subtropical dry forest

The subtropical dry forest region is located on the south-southwestern side of Puerto Rico in the shadow of the

central mountains with annual rainfall totals less than 1,000 mm. The dry forests in Puerto Rico are small in stature, and they have low diversity, productivity, and above ground biomass (Murphy *et al.*, 1995). Dry forests will likely be sensitive to future changes in rainfall,

which will also likely alter species distribution and ecosystem processes within this forest system (Allen *et al.*, 2017).

Figure 3 shows distributions of monthly average daily minimum and maximum temperature from the historical
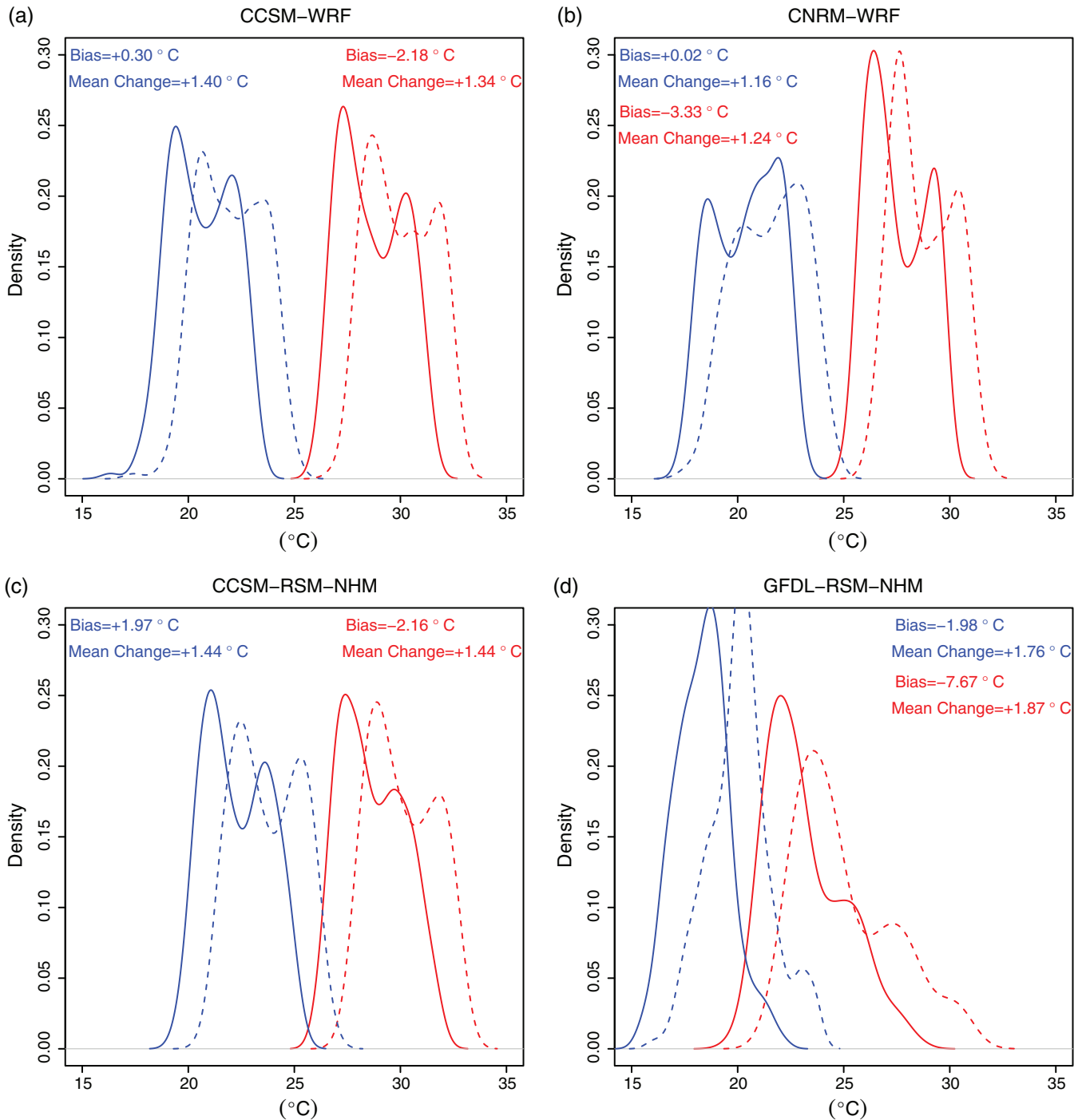
FIGURE 3 Distributions of monthly averaged daily maximum (red) and minimum (blue) 2-m temperature for the subtropical dry forest. The historical and future are shown as solid and dashed lines respectively for (a) CCSM-WRF, (b) CNRM-WRF, (c) CCSM-RSM-NHM, d) GFDL-RSM-NHM. Included in each panel are the annual averaged bias and the mean change. The projected changes are all significant at the 95% confidence level using the Mann–Whitney *U*-test (*p*-values < .001)

TABLE 2 Maximum and minimum 2-m temperature bias and change for each high-resolution RCM simulation averaged over the dry Forest (DF), moist Forest (MF) and wet Forest (WF)

GCM	TMIN bias (°C)			TMAX bias (°C)			TMIN change (°C)			TMAX change (°C)		
	DF	MF	WF	DF	MF	WF	DF	MF	WF	DF	MF	WF
CCSM-WRF	+0.30	+0.17	+0.41	−2.18	−2.50	−2.79	+1.40	+1.36	+1.34	+1.34	+1.56	+1.70
CCSM-RSM-NHM	+1.97	+1.48	+1.36	−2.16	−2.86	−3.39	+1.44	+1.48	+1.39	+1.44	+1.47	+1.56
CNRM-WRF	+0.02	-0.19	+0.13	−3.33	−3.06	−3.39	+1.16	+1.18	+1.13	+1.25	+1.14	+1.16
GFDL-RSM-NHM	-1.98	−2.04	−1.74	−7.67	−8.23	−8.81	+1.76	+1.63	+1.52	+1.87	+1.75	+1.65

and RCP8.5 regional climate model realizations averaged over the subtropical dry forest. Figure 3 includes the model biases relative to PRISM and the mean projected changes for both maximum and minimum temperature. Both WRF simulations have the smallest bias (less than <0.3°C) for minimum temperature. In comparison the RSM-NHM minimum temperature bias is approximately +2.0°C for the downscaled CCSM simulation and − 2.0°C for the GFDL simulation. The GFDL simulation downscaled using RSM-NHM depicts a very different shape in the distribution of both minimum and maximum temperatures with a maximum temperature bias of −7.6°C. In particular, the temperature distribution for the GFDL-RSM-NHM simulation does not display the characteristic bimodality as found in the other realizations, which is found within the observations (not shown). The large cold bias in the maximum temperatures for the GFDL-RSM-NHM simulation is concerning and will be discussed in more detail when looking at precipitation errors. There is also a cold bias for maximum temperature for the other three downscaled realizations, but those biases are smaller, ranging from −2.2°C to −3.3°C. In general, the downscaled simulations have a warm bias at night and a cold bias during the day, and this persists between regions as seen in Table 2. The cold bias during the day may be a direct result of the SSTs. The downscaled realizations use SSTs from the driving global model, and SST in each of these models has a cool bias compared to observations within this region (see figure 4 of Ryu and Hayhoe, 2014). Additionally, there is also a larger diurnal temperature range for the WRF simulations compared to the RSM-NHM simulations. As for the projected changes, the change for WRF exceeds the model bias with mean increases in minimum temperature of 1.4°C and 1.2°C for the CCSM and CNRM realizations, respectively. The CCSM downscaled with RSM-NHM projects comparable changes to minimum temperatures of 1.4°C, despite the larger bias. The mean increase for maximum temperature for CCSM-WRF, CCSM-RSM-NHM, and CNRM-WRF is between 1.2 and 1.4°C, comparable to that for

minimum temperature. Accordingly, the diurnal cycle within the subtropical dry forest is projected to be largely unchanged (Figure S1).

Alarmingly, unprecedented heat may prevail throughout the subtropical dry forest by 2050. Figure 4 shows the number of days per year that are projected to exceed the warmest day in the historical simulation for maximum and minimum temperature. This analysis examines each calendar day in the 20-year historical period and determines the maximum temperature for that day from the hourly model output. Then, the temperatures for each calendar day in the future period is compared against the maximum for the same calendar day from the 20-year historical period to determine the number of exceedances of the historical maximum at each grid point within the subtropical dry forest. An average is calculated for all grid points within the subtropical dry forest. Figure 4 shows the number of exceedances for each of the future years, which illustrates the interannual variability in the number of days that exceed the historical baseline for minimum and maximum temperatures. The median from all the realizations generally exceeds 100 days per year with for both maximum and minimum temperature. All realizations indicate exceptional years with more than 150 days for both maximum and minimum temperatures. We also note larger consistency between the downscaled realizations for minimum temperatures compared to maximum temperatures. Considering that the mean change for both mean maximum and minimum temperature is <1.5°C within the island, which is the goal of the Caribbean Community (Taylor and Clarke, 2018), these results highlight unprecedented temperature extremes throughout the year. Having daily future maximum and minimum temperatures in the future exceed the historical baseline more than 100 times per year will create significant stress on both the subtropical dry forest ecosystem and people in this region.

There is some consensus on how mean precipitation will evolve within the subtropical dry forest as

FIGURE 4 Boxplot of the annual count of days within the subtropical dry forest of Puerto Rico for each future year when the daily (a) maximum 2-m temperature and (b) minimum 2-m temperature exceeds the same calendar day maximum temperature from the historical period for each RCM simulation. The number of days is averaged over the subtropical dry forest. The projected changes are significant at the 95% confidence level using the Mann–Whitney U-test (p-values < .001)
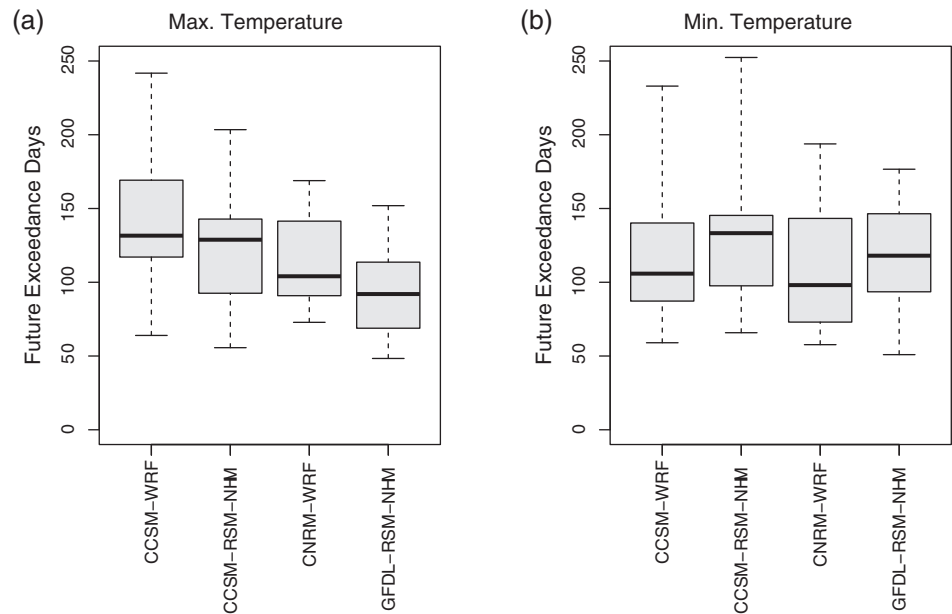
GHGs increase. Figure 5 shows the distribution of monthly precipitation for both the historical period and RCP8.5. There is a dry bias in both WRF simulations and in the CCSM-RSM-NHM simulation. The bias is larger for the CCSM simulations from both regional climate models and smallest for CNRM-WRF simulation. Notably, CCSM-WRF is the only simulation that does not simulate rainfall exceeding 200 mm month^{-1}. These results illustrate that using different global and regional models increases uncertainty for precipitation extremes in this region. Despite differences in the distributions, CCSM-WRF, CNRM-WRF, and CCSM-RSM-NHM reflect a reduction in mean rainfall between 18–20%. The mean changes in CNRM-WRF and CCSM-RSM-NHM are more sensitive to changes in extreme rainfall compared to CCSM-WRF. GFDL-RSM-NHM was omitted from this analysis because this simulation includes a very large wet bias, exceeding 100 mm month^{-1}, as well as the strong cold bias previously discussed.

The hourly model output enables quantifying changes to sub-daily precipitation, including the diurnal cycle and short-duration precipitation extremes. Precipitation extremes, here defined as events when the daily maximum precipitation rate (mm hr^{-1}) exceeds the 99th percentile of the historical period, are shown in Figure 6. These results indicate that the projected change in the frequency of extreme rainfall events is insignificant when averaged over the life zone. Figure 6 further suggests that the frequency of flash flooding (resulting directly from extreme precipitation) may not change in the absence of tropical storms and hurricanes, which are poorly simulated in our limited domain. However, flash flooding events could increase if there are larger gaps between precipitation events because of a drier land surface which would favour quicker run-off.

There are also notable projected changes in the diurnal cycle (Figure 7). Except for GFDL-RSM-NHM, the models show a consistent rainfall peak during the afternoon/evening hours in both the historical period and RCP8.5. One characteristic of the projected drying within the subtropical dry forest is a reduction in afternoon/evening rainfall, likely from convection. The major difference between RSM-NHM and the WRF simulations is the timing of the peak rainfall, occurring later in the evening for RSM-NHM.

3.1.1 | Puerto Rico—subtropical moist forest

The subtropical moist forest region is primarily located in transition zone between the coast and higher elevations with a more concentrated moist forest area on the north and east side of the island (Figure 1). Annual rainfall totals are typically 1,000–2000 mm. This is the largest life zone, covering around 59% of Puerto Rico, and it is a prime region for deforestation because climatic conditions are ideal for growing a variety of crops (Miller and Lugo, 2009). The subtropical moist forest includes many microhabitats with very diverse species. For instance, the karst region on the northern edge of Puerto Rico harbours more than 1,300 species of plants and animals (Lugo *et al*., 2001). Climate change poses a risk to the ecosystems and ecosystem services, such as shade-grown coffee, in these subtropical moist forests.
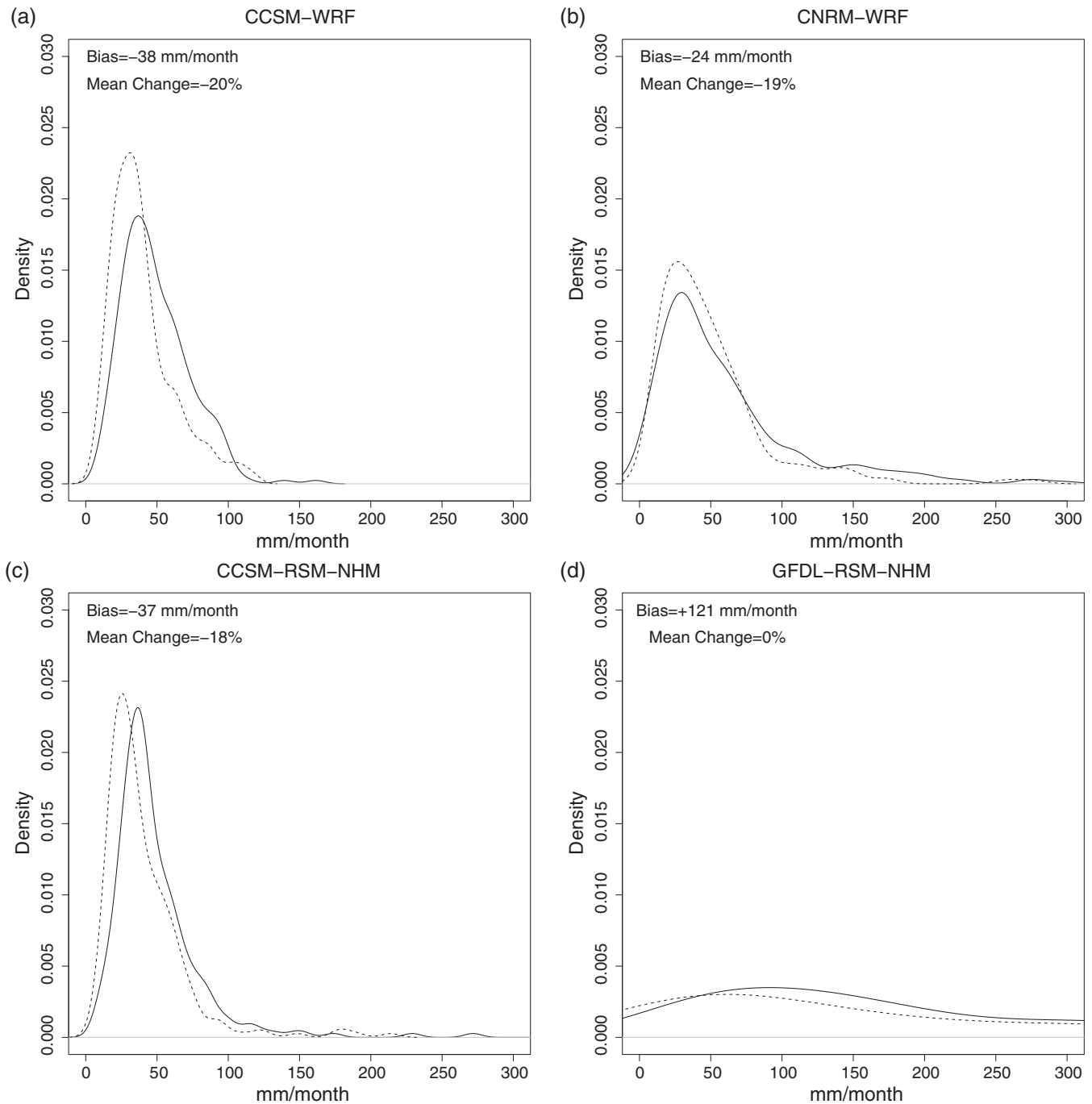
FIGURE 5 Distribution of monthly precipitation (mm) for the subtropical dry forest region. The historical and future are shown as solid and dashed lines respectively for (a) CCSM-WRF, (b) CNRM-WRF, (c) CCSM-RSMNHM, (d) GFDL-RSM-NHM. Included in each panel are the annual average bias relative to PRISM and the annual mean change. Except for GFDL-RSM-NHM (*p*-value = .543), the projected changes are significant at the 95% confidence level using the Mann–Whitney *U*-test (*p*-values < .001)

Figure 8 shows distributions of daily average minimum and maximum temperature from the downscaled simulations. Similar to the dry forest, see Table 2 for regional comparison, the WRF simulations have the smallest minimum temperature biases of ±0.2°C relative to PRISM. In comparison, the RSM-NHM minimum temperature bias is approximately +1.2°C for the downscaled CCSM simulation and − 2.0°C for the GFDL simulation. Excluding the GFDL-driven simulation, the simulated maximum temperature bias is between −2.5°C and −3.1°C. The projected change for both WRF simulations and CCSM-RSM-NHM exceed the model bias with a projected increase in minimum temperature of 1.2–1.5°C. The projected increase in
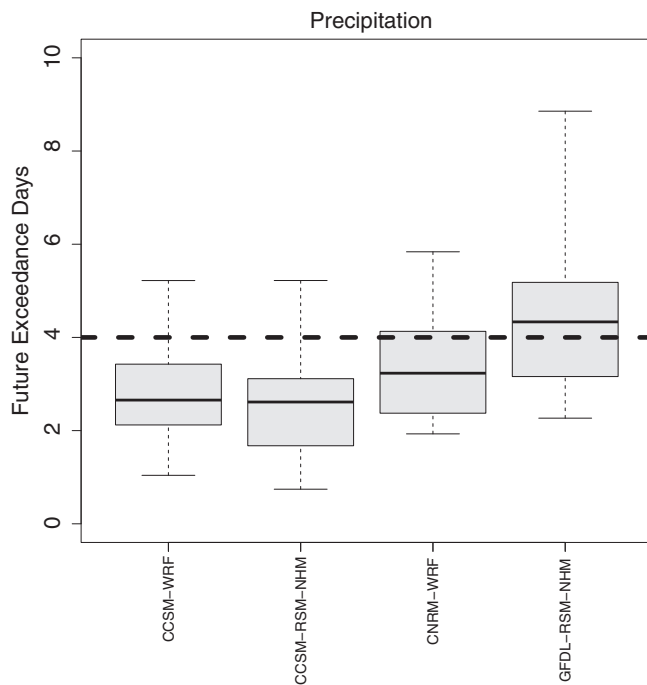
Precipitation

FIGURE 6 Boxplot of the annual count of days for each future year when the daily maximum precipitation rate (mm hr-1) exceeds the 99th percentile of the historical period for each RCM simulation. The number of days is averaged over the subtropical dry forest. The average historical annual count of days per year that exceed the 99th percentile is 4 days (dashed horizontal line)

maximum temperature ranges from 1.1 to 1.6°C. The range of projected temperature change is larger for the subtropical moist forest relative to the subtropical dry forest. There is more uncertainty in the mean warming within the subtropical moist forest compared to the subtropical dry forest, which is associated with a weaker consensus in the projected change in the diurnal temperatures (Figure S2).

Figure 9 shows the number of days per year that exceed the warmest day in the historical simulation on average for the subtropical moist forest. CNRM-WRF has a mean temperature change of 1.1°C with a median of 100 days of unprecedented heat per year, while CCSM-WRF projects a mean change of 1.6°C and > 150 days per year, which illustrates how small changes in the projected mean temperature can result in extreme heat given the small daily temperature variability in a tropical climate. All simulations project at least 50 days per year of unprecedented temperatures at 2050 relative to the historical period. Overall, downscaled model projections for the largest life zone in Puerto Rico indicate a significant change in unprecedented heat with some projections exceeding 200 days for some future years.

Figure 10 is the distribution of monthly precipitation for the historical and RCP8.5 simulations. As anticipated, annual rainfall totals are larger for the subtropical moist forest compared to the subtropical dry forest, see Table 3 for regional comparison, but there remains consistent dry bias of −19 mm month^{-1} to −44 mm month^{-1}. The outlier is the extreme wet bias in GFDL-RSM-NHM, exceeding 200 mm month^{-1}. The WRF precipitation biases are smaller than the other models. The simulation with the smallest bias is CCSM-WRF, which has the largest projected reduction in annual rainfall (23%). The CNRM-WRF simulation projects the smallest reduction (9%). The CCSM-RSM-NHM simulation despite having a larger bias is in between the two WRF simulations, annual rainfall reduced by 17%. The CCSM-WRF and CCSM-RSM-NHM project the largest reduction in precipitation, suggesting a stronger sensitivity to the driving global climate model than the regional climate model. Overall, there is greater uncertainty in the magnitude of change within the subtropical moist forest relative to the subtropical dry forest.

There is a slight reduction in the number of days per year with extreme rainfall qualitatively like the subtropical dry forest (Figure S3). There is also a consistent projected reduction in the afternoon and evening rainfall (Figure S4), as in the subtropical dry forest. Overall, there is consistency between sub-daily changes in the diurnal cycle and precipitation extremes between the subtropical moist forest and subtropical dry forest for different global and regional climate models.

3.1.2 | Subtropical wet Forest

The subtropical wet forest region is found in much of the higher elevations within Puerto Rico (Figure 1). This life zone has high annual rainfall totals of 2000–4,000 mm. Abundant precipitation supports lush vegetation and a high diversity of species. The runoff from the subtropical wet forest is an important source of freshwater for populations near the coastal areas (Miller and Lugo, 2009).

Figure 11 shows distributions of daily average minimum and maximum temperatures from the historical and RCP8.5 regional climate model realizations. Predictably, GFDL-RSM-NHM remains an outlier, so it is not discussed. The remaining simulations have a warm bias for minimum temperature. CCSM-RSM-NHM has the largest warm bias for minimum temperature of 1.4°C compared to 0.4°C and 0.1°C for CCSM-WRF and CNRM-WRF, respectively. The smaller bias in WRF for minimum temperature is consistent with the other life zones. Maximum temperature is biased cold, ranging
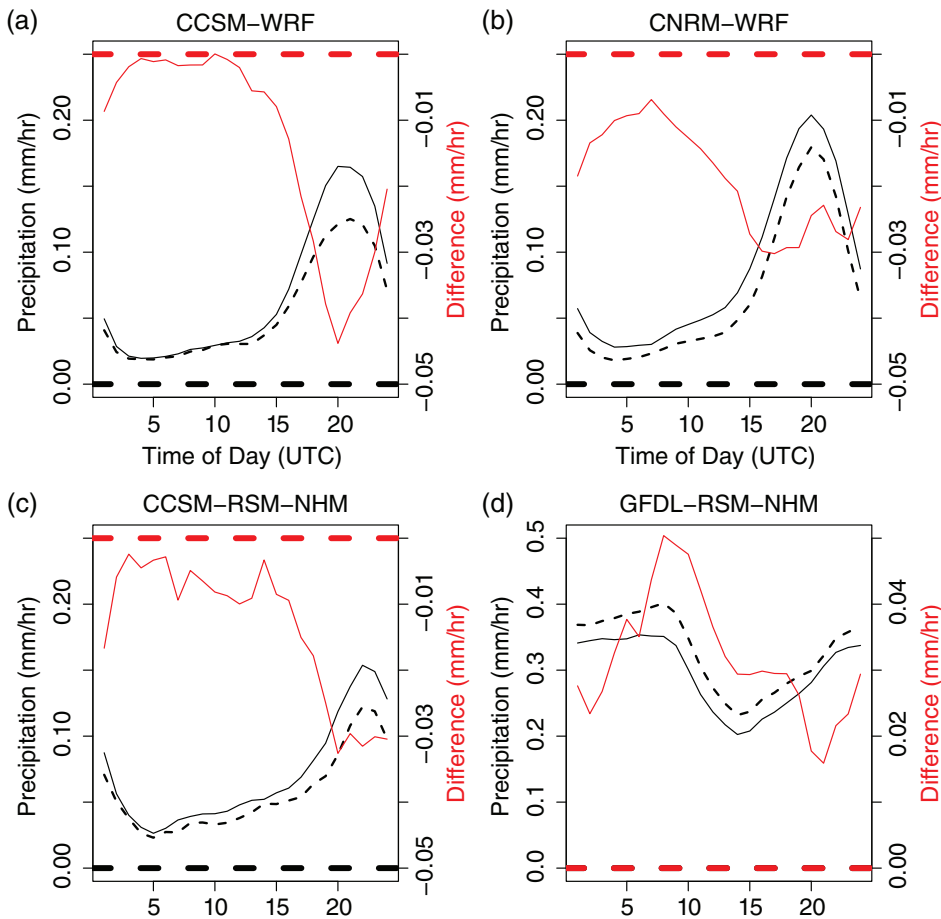
FIGURE 7 Diurnal cycle of precipitation (mm hr-1) for the subtropical dry forest. The historical and future are shown as black solid and dashed lines with precipitation difference in red respectively for (a) CCSM-WRF (p-value = .004), (b) CNRM-WRF (p-value < .001), (c) CCSM-RSM-NHM (p-value < .001), (d) GFDL-RSM-NHM (p-value = .363). Note the plotted range for precipitation for GFDL-RSM-NHM is substantially larger than the other simulations

from −2.8°C for CCSM-WRF to −3.4°C for both CNRM-WRF and CCSM-RSM-NHM. The cooler daytime temperatures and warmer night-time temperatures indicate the regional climate models are consistently underestimating the diurnal temperature range across different life zones. The projected change from the three realizations depict an increase in minimum temperature of 1.1–1.4°C and 1.2–1.7°C for maximum temperature. The projected maximum temperature changes are slightly larger than the minimum temperature change, especially for CCSM-WRF. The projected change in the diurnal cycle confirms that maximum temperature increases more during the afternoon and evening hours for CCSM-WRF compared to CNRM-WRF and CCSM-RSM-NHM (Figure 12), and hence escalating uncertainty in changes to the diurnal temperature range. Similar to the other life zones, there is a substantial projected increase in unprecedented daytime and night-time temperatures exceeding 200 days for some future years (Figure S4).

Figure 13 shows the distribution of monthly precipitation from the historical and RCP8.5 simulations averaged over the subtropical wet forest. The simulations all show a dry bias, except for GFDL-RSM-NHM. CNRM-WRF has the smallest bias (−21 mm month^{-1}), as well as the smallest mean future rainfall decrease (10%). The CCSM-WRF and CCSM-RSM-NHM have dry biases of 26 mm month^{-1} and 56 mm month^{-1} and mean decreases of 25% and 16%, respectively. Notably, the simulation with the smallest bias differs for each life zone. Consistent with temperature, the uncertainty in the magnitude of the drying becomes larger for the wetter life zones, see Table 3 for regional comparisons. This is likely because there is more uncertainty as the representation of clouds and precipitation become increasingly important for wetter regions. The increased uncertainty is likely associated with local feedbacks in the model such as evapotranspiration and recycling of water. For instance, comparing projected changes in the diurnal temperature and precipitation (Figures 12 and 14) provides some insight. CCSM-WRF has the largest amount of drying and associated with larger decrease in afternoon precipitation. The reduced afternoon precipitation favours a relative increase in temperature. On the other hand, CNRM-WRF has a smaller amount of drying and associated with a smaller reduction in afternoon precipitation. The smaller projected change to afternoon
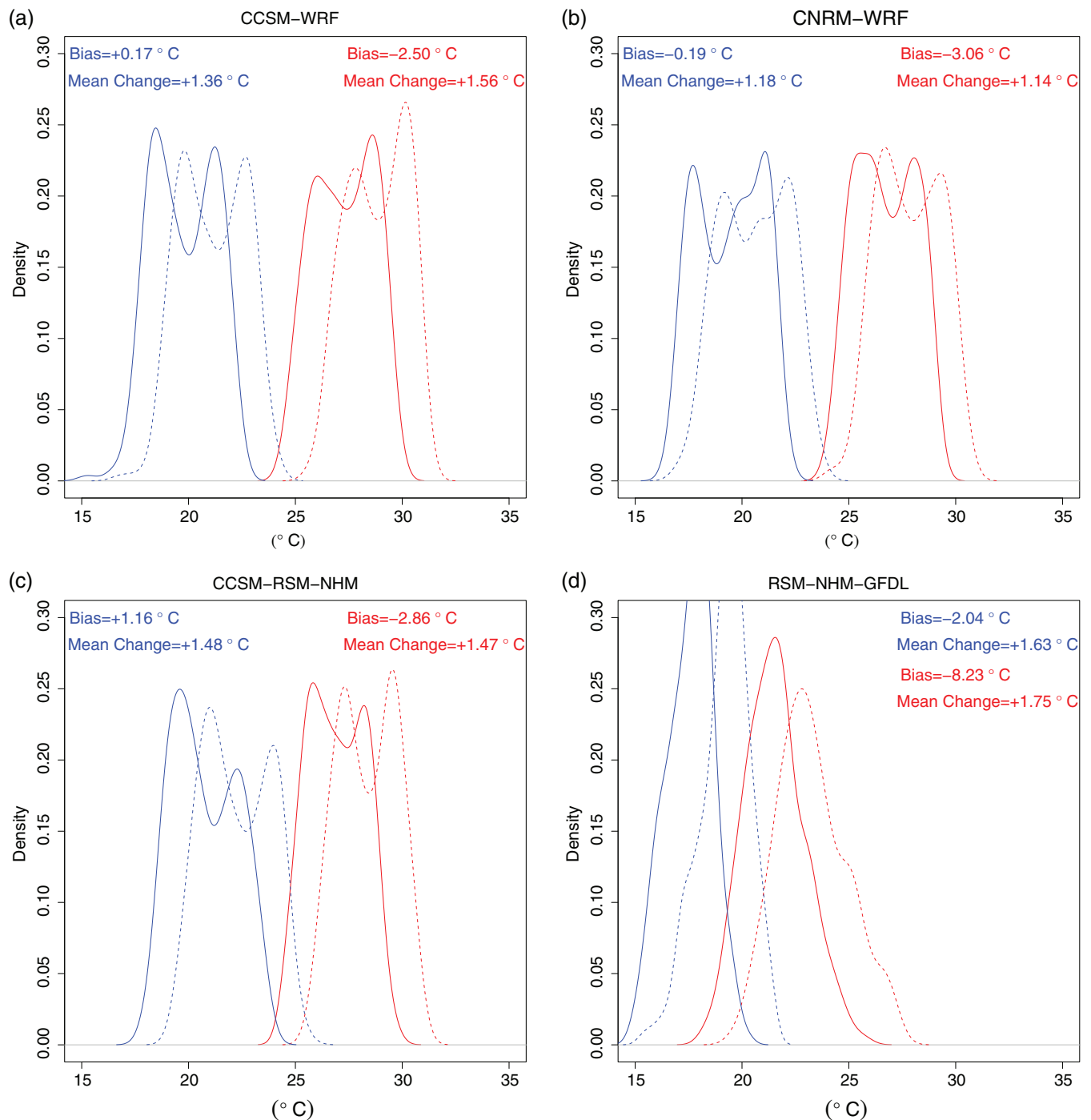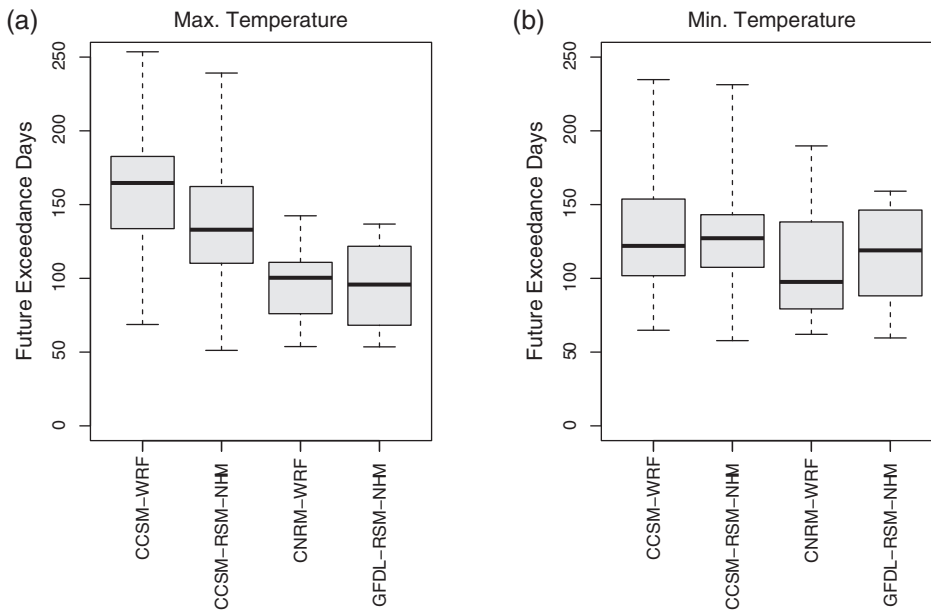
FIGURE 8 Same as Figure 3, except for the subtropical moist forest. The projected changes are significant at the 95% confidence level using the Mann–Whitney *U*-test (*p*-values < .001)

precipitation is associated with less warming during the afternoon. The larger projected reduction in precipitation in CCSM-WRF reflects a more pronounced decrease in the frequency of extreme rainfall events (Figure S5) compared to CNRM-WRF. Such details in the local physical processes are important to understand and are currently being explored for a future manuscript.

3.2 | U.S. Virgin Islands

The U.S. Virgin Islands (St. Thomas, St. John, and St. Croix) generally have subtropical dry forests at lower elevations and subtropical moist forests at higher elevations (Brandeis *et al.*, 2009). The within-island climate gradient is largest for St. Croix, the largest of the U.S. Virgin Islands, with a notable transition in forest

FIGURE 9 Same as Figure 4, except for the subtropical moist forest. The projected changes are significant at the 95% confidence level using the Mann–Whitney U-test (p-values < .001)

type from subtropical dry forests on the eastern/southern side of the island to subtropical moist forests on the northwest side of the island. Below we focus only on the WRF simulations because these simulations themselves provide insight into some consistencies but more importantly uncertainties in the model projections.

Figure 15 shows the simulated annual average maximum temperature from the WRF simulations compared to the station climate normals. Both WRF simulations illustrate larger maximum temperatures over land at the lowest elevations, but the magnitude is cooler than the station observations by 1 to 3°C. As for minimum temperatures, the largest cooling is found at the higher elevations but there is also a notable cold bias (Figure S6). Figure 16 shows the simulated historical annual rainfall totals from the WRF simulations compared to the station climate normals. The models simulate a distinguishable windward-leeward effect. The annual rainfall climatology in CNRM-WRF is closer to observations compared to CCSM-WRF, which has a notable wet bias on the windward side of the islands. Despite the wet bias in CCSM-WRF, the within island rainfall spatial characteristics are similar to that of CNRM-WRF. The station observations show similar windward-leeward rainfall characteristics. The exception is the drier climate for the far eastern edge of St. Croix, which is unresolved at 2-km horizontal grid spacing.

The island average projected change in the maximum temperatures is 1.1–1.3°C for CNRM-WRF and CCSM-WRF, respectively (Figure 17). The within-island temperatures are projected to increase faster than the surrounding water. There are some intriguing similarities between the simulations in the placement

of the largest projected warming for maximum temperatures. There is larger warming on the southern side at lower elevations within St. Croix and for some of the highest elevations within St. Thomas and St. John. Similar spatial changes are seen for minimum temperature (Figure S7).

The projected decrease in the annual precipitation for the U.S. Virgin Islands is 6–12% (Figure 18), which is less than in life zones of Puerto Rico. Unlike the temperature projections which indicate similar locations for the maximum increase in temperatures, the rainfall projections are not in agreement for the location of the largest projected reductions in precipitation. CNRM-WRF projects more drying on the southern (leeward side) of the islands, while CCSM-WRF shows the largest drying on the northern (windward side). These results suggest that the model biases translate into differential climate sensitivity. For instance, the largest precipitation reductions on the windward side of the islands for CCSM-WRF are co-located with a larger wet bias. Overall, these results emphasize the uncertainty in projected changes across the U.S. Virgin Islands and demonstrate that projected precipitation changes are unlikely to be uniform.

4 | CONCLUSIONS AND DISCUSSION

The dynamically downscaled simulations in this study provide additional information by resolving precipitation gradients between life zones and of significant value to those interested in climate change for the islands. All simulations project substantial increases in
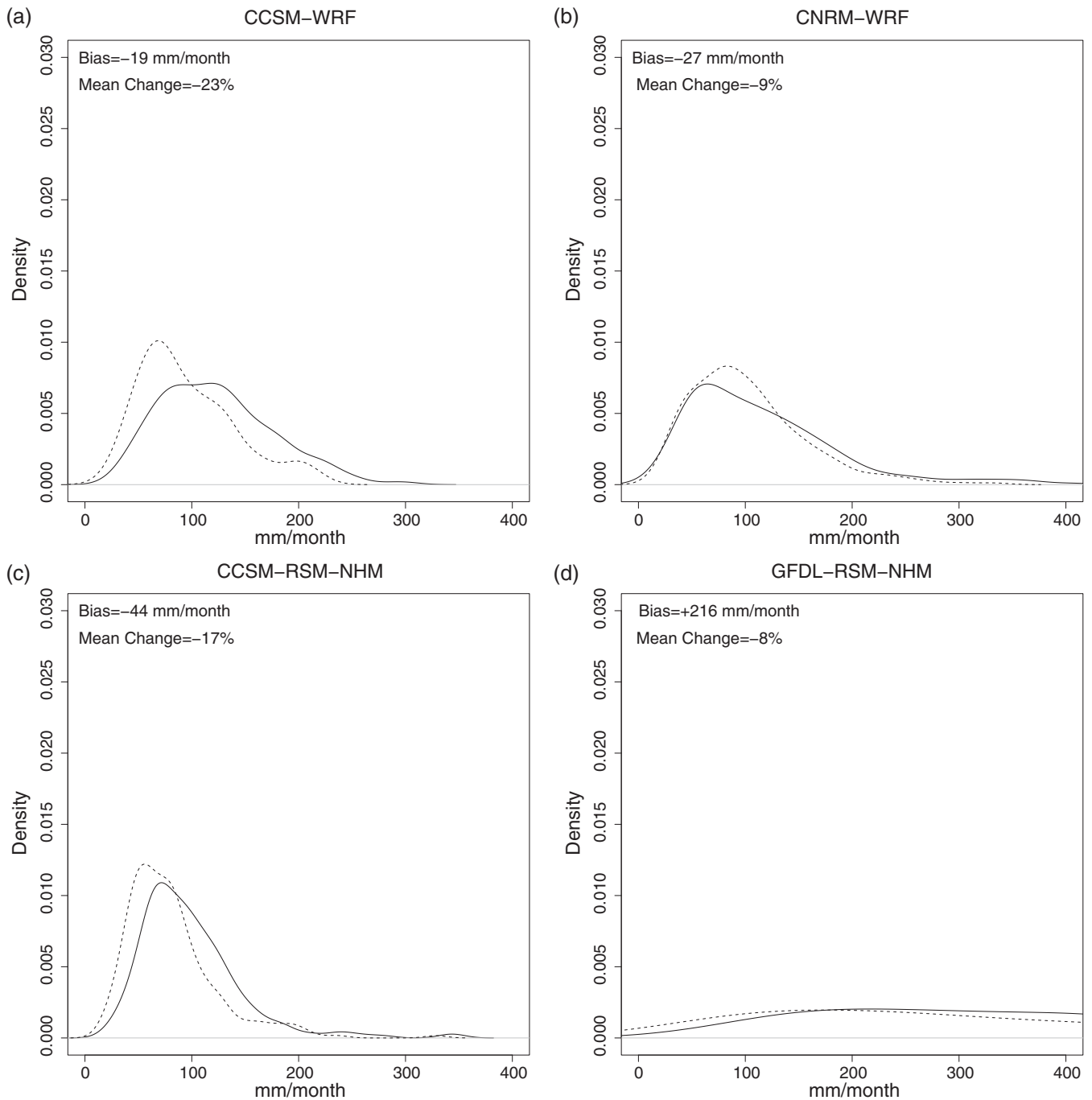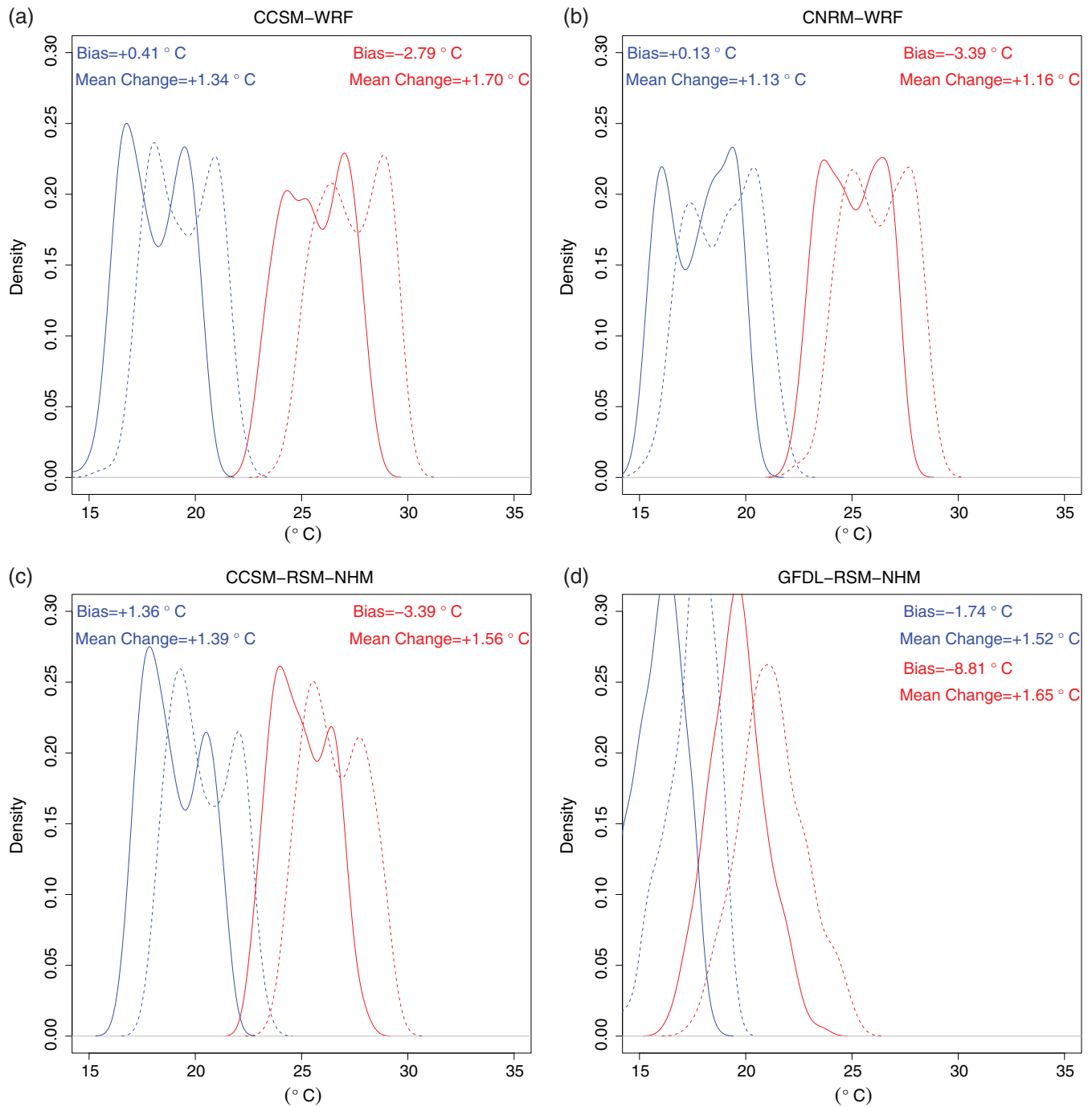
FIGURE 10 Same as Figure 5, except for the subtropical moist forest. Except for GFDL-RSM-NHM (*p*-value = 0.05), the projected changes are significant at the 95% confidence level using the Mann–Whitney *U*-test (*p*-values. < .001)

TABLE 3 Precipitation bias and change for each high-resolution RCM simulation averaged over the dry Forest (DF), moist Forest (MF), and wet Forest (WF)

GCM	Precip. bias (mm/month)			Precip. change (%)		
	DF	MF	WF	DF	MF	WF
CCSM-WRF	−38	−19	−26	−20	−23	−25
CCSM-RSM-NHM	−37	−44	−56	−18	−17	−16
CNRM-WRF	−24	−27	−21	−19	−9	−10
GFDL-RSM-NHM	+121	+216	+232	0	−8	−6

(a) CCSM–WRF

Bias=+0.41 °C
Mean Change=+1.34 °C

Bias=−2.79 °C
Mean Change=+1.70 °C

(b) CNRM–WRF

Bias=+0.13 °C
Mean Change=+1.13 °C

Bias=−3.39 °C
Mean Change=+1.16 °C

(c) CCSM–RSM–NHM

Bias=+1.36 °C
Mean Change=+1.39 °C

Bias=−3.39 °C
Mean Change=+1.56 °C

(d) GFDL–RSM–NHM

Bias=−1.74 °C
Mean Change=+1.52 °C

Bias=−8.81 °C
Mean Change=+1.65 °C

FIGURE 11 Same as Figure 3, except for the subtropical wet forest. The projected changes are significant at the 95% confidence level using the Mann–Whitney U-test (p-values < .001)

temperature and decreases in precipitation for all life zones within Puerto Rico by 2050. In the subtropical dry forest, more persistent mean annual warming (1.2–1.4°C) and persistent drying (reduction in mean annual rainfall 18% to–20%) is projected. However, the dynamically downscaled simulations suggest increased uncertainty in the mean warming and drying for the wetter life zones. For the moist forest, the mean

projected warming is 1.1–1.6°C, while the wet forest is 1.1–1.7°C. The mean precipitation is projected to reduce by 9–23% in the subtropical moist forest and 10–25% in the subtropical wet forest. Current research is underway to better understand the physical drivers with unknown effects on the mean change, especially precipitation, for the wetter life zones within Puerto Rico. Notably, the wetter life zones are found at higher

FIGURE 12 Average diurnal cycle of temperature (°C) for the subtropical wet forest. The historical and future are shown as black solid and dashed lines with temperature difference in red respectively for (a) CCSM-WRF, (b) CNRM-WRF, (c) CCSM-RSM-NHM, (d) GFDL-RSM-NHM. The plotted range for temperature is colder for GFDL-RSM-NHM-GFDL than for the other simulations. The projected changes are significant at the 95% confidence level using the Mann–Whitney U-test (p-values < .001)
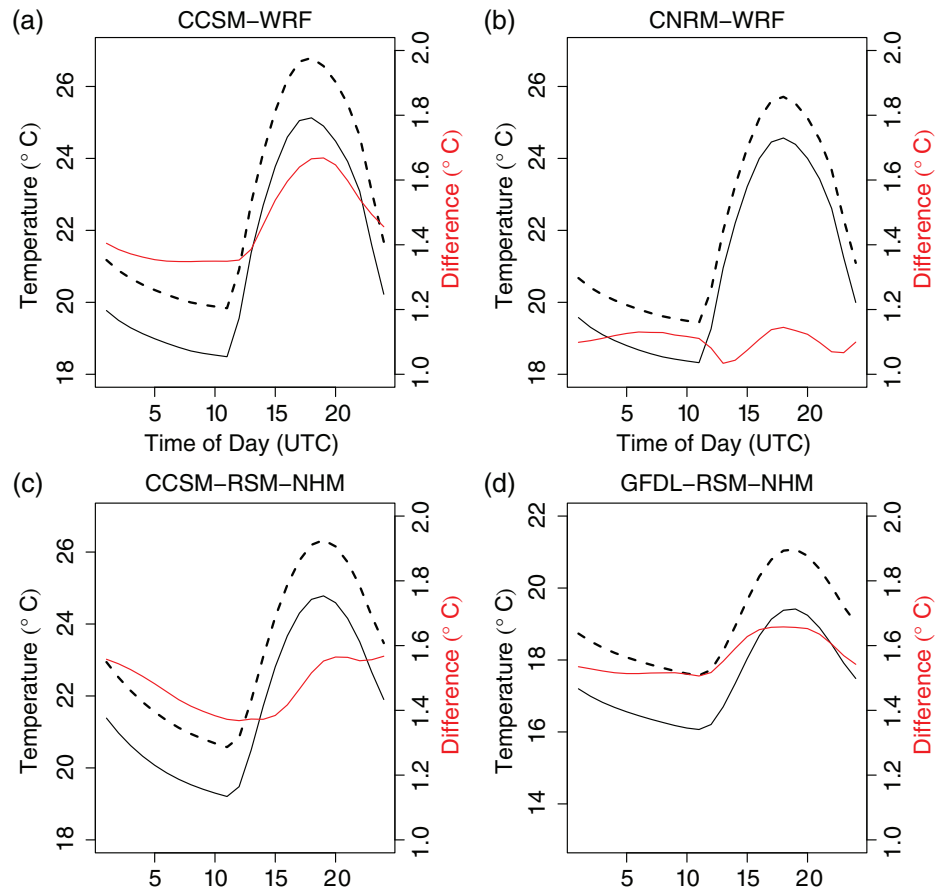
elevations, which suggests a possible "elevation buffer" to the subtropical precipitation decline. The existence of this feature would alter local climate change adaptation efforts within the island.

For all life zones within Puerto Rico, a mean warming well below 2°C—a global warming target—results in marked increases in minimum and maximum temperatures at 2050 relative to the historical period. As such, all simulations project more than 50 days of unprecedented maximum and minimum temperatures in each future year with some exceptional years exceeding 200 days. The simulations also agree that there are small changes in the frequency of extreme rainfall within Puerto Rico for all life zones at 2050. This study corroborates Bhardwaj et al. (2018) in that changes to extreme rainfall frequency are robust and not sensitive to driving model, the regional climate model, or the regional climate model configuration. However, the dynamically downscaled extreme rainfall frequency projections differ from the statistically downscaled projections for Puerto Rico (Hayhoe, 2013). We hypothesize that the difference between the two downscaling methods results from simulating the complex feedbacks associated with competing drivers of change, the dynamic contribution that

supports more drying and the thermodynamic contribution that supports an increase in the atmosphere moisture capacity and extreme rainfall (Pfahl et al., 2017). Hence, more work is needed to understand differences between high-resolution dynamical downscaled simulations that are at similar spatial scales as that of statistical downscaling, especially for places with fewer observations.

The projected warming for the U.S. Virgin Islands (1.1–1.4°C) is comparable to Puerto Rico. The downscaled simulations depict the largest maximum temperature change for the southern side of St. Croix and for some of the higher elevations within St. Thomas and St. John. The simulations also project a reduction in mean annual rainfall of 6–12% for the islands, which is smaller than for Puerto Rico. However, unlike for temperature, there is considerable uncertainty in the location of the maximum drying (e.g., more drying for the windward or leeward side of the islands).

Finally, this study highlights modelling challenges for traditional dynamical downscaling of global climate models for the U.S. Caribbean. One consistent issue is a cold bias for all life zones within Puerto Rico and for the U.S. Virgin Islands. The cold bias is persistently larger for
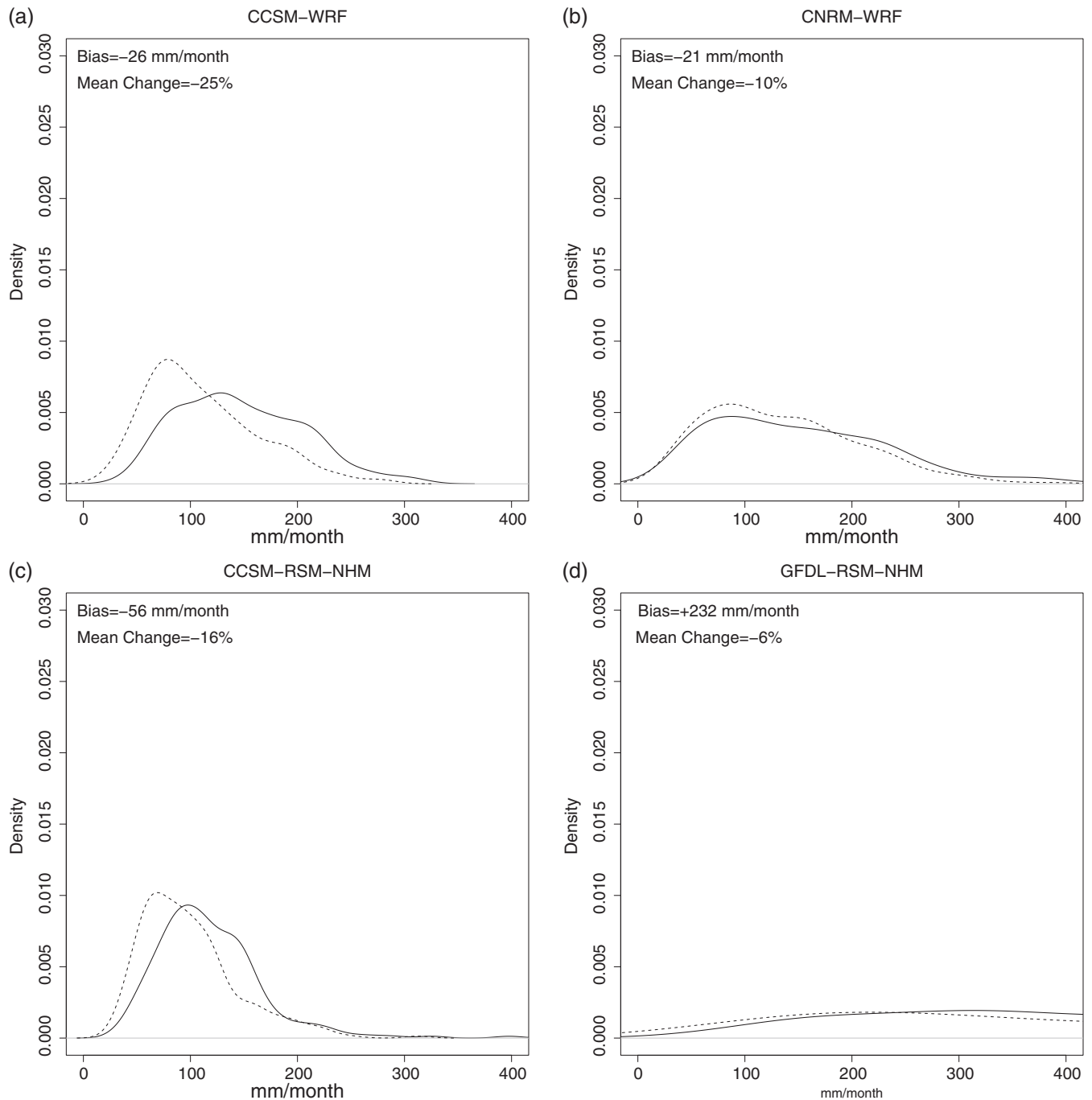
FIGURE 13 Same as Figure 5, except for the subtropical wet forest. With the exception of RSM-NHM-GFDL (*p*-value = 0.05), the projected changes are significant at the 95% confidence level using the Mann–Whitney *U*-test (*p*-values < .001)

maximum temperatures compared to minimum temperatures. There is also a persistent dry bias for all simulations within Puerto Rico except GFDL-RSM-NHM. With traditional dynamical downscaling, the global model biases remain, such as a cold SST bias that was acquired from the global climate model SSTs. The cold bias in SST helps to explain the cold bias in near surface temperature within the islands, which may also be contributed to a

persistent dry bias within Puerto Rico. For instance, a warmer Atlantic is associated with increased convection, especially during the rainy season (Wang *et al.*, 2008). The regional climate model's performance does not discredit the future runs and projected changes (Santer *et al.*, 2009; Knutti *et al.*, 2010), but it limits some interpretations and raises some important questions that can may help improve model performance. For instance, the

FIGURE 14 Same as Figure 7, except for the subtropical wet forest; (a) CCSM-WRF (*p*-value < .001), (b) CNRM-WRF (*p*-value = .484), (c) CCSM-RSM-NHM (*p*-value < .001), (d) GFDL-RSM-NHM (*p*-value = .036)
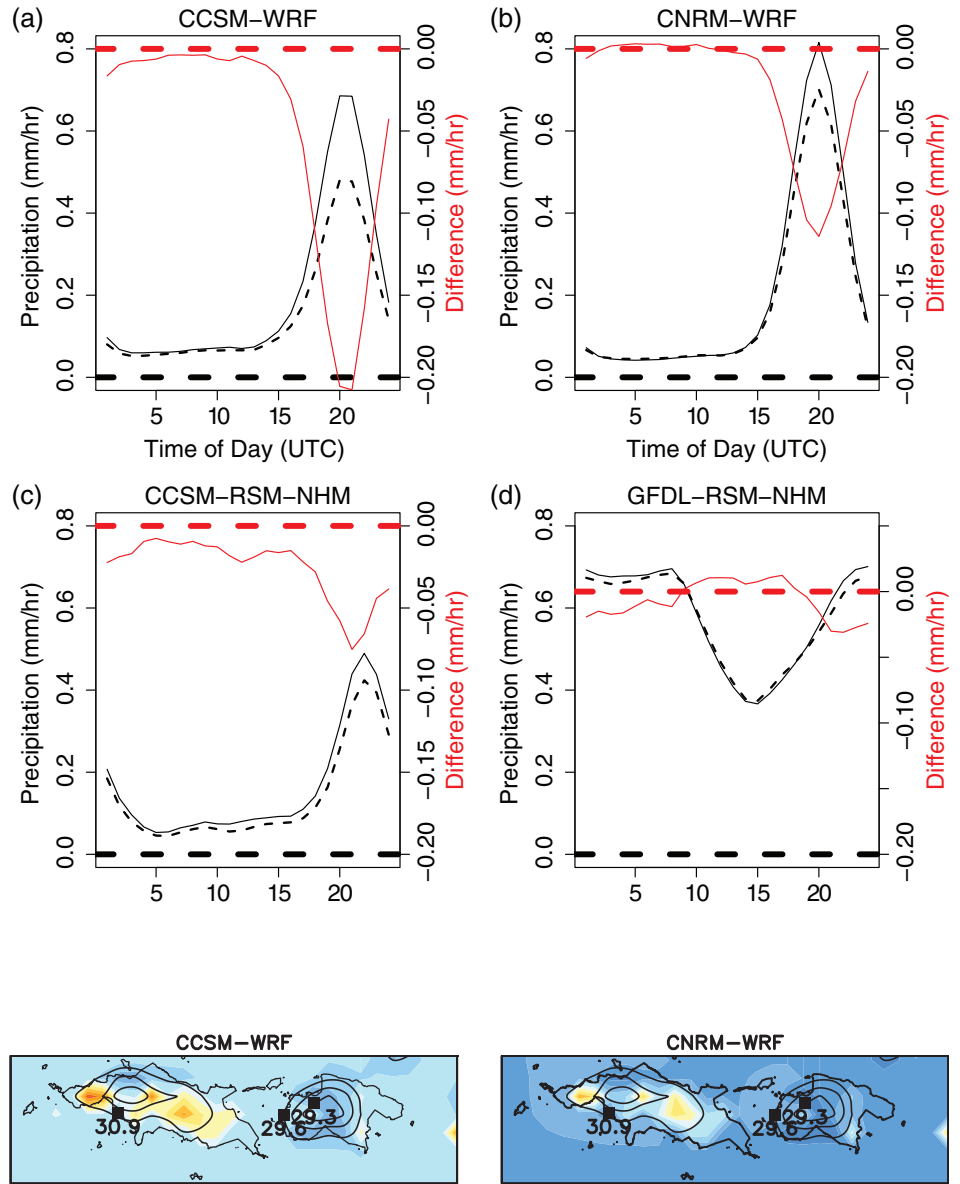
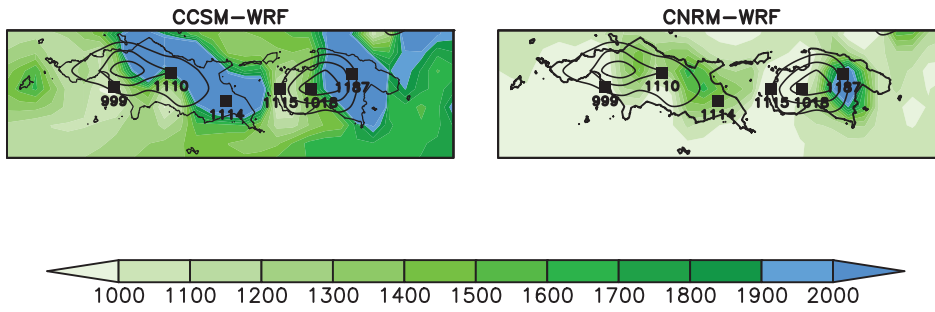**FIGURE 15** Annual average maximum temperature (°C) for St. Thomas and St. John (top) and St. Croix (bottom) from the WRF historical climatology (1986-2005) with weather station climate normals (1981-2010) overlaid in text. Contours represent the model elevation starting with the first contour at 50 m (not labelled)
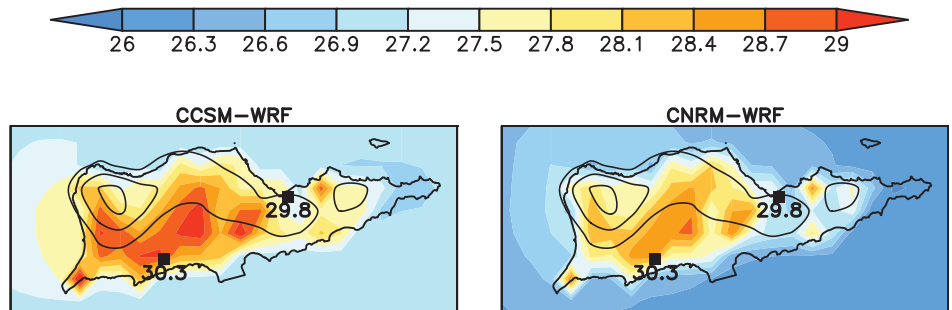
presence of a cold and dry bias can adversely affect threshold statistics of ecological relevance, such as the number of days above 32°C or daily precipitation exceeding 25 mm. While the cold bias in SST raises questions on its influence on the dynamically downscaled projections. Follow-on research will explore the cold bias in SST to better understand the impact on the projected changes.

FIGURE 16 Annual precipitation (mm) for St. Thomas and St John (top) and St. Croix (bottom) from the WRF historical climatology (1986-2005) with weather station climate normals (1981-2010) overlaid in text. Contours represent the model elevation starting with the first contour at 50 m (not labelled)
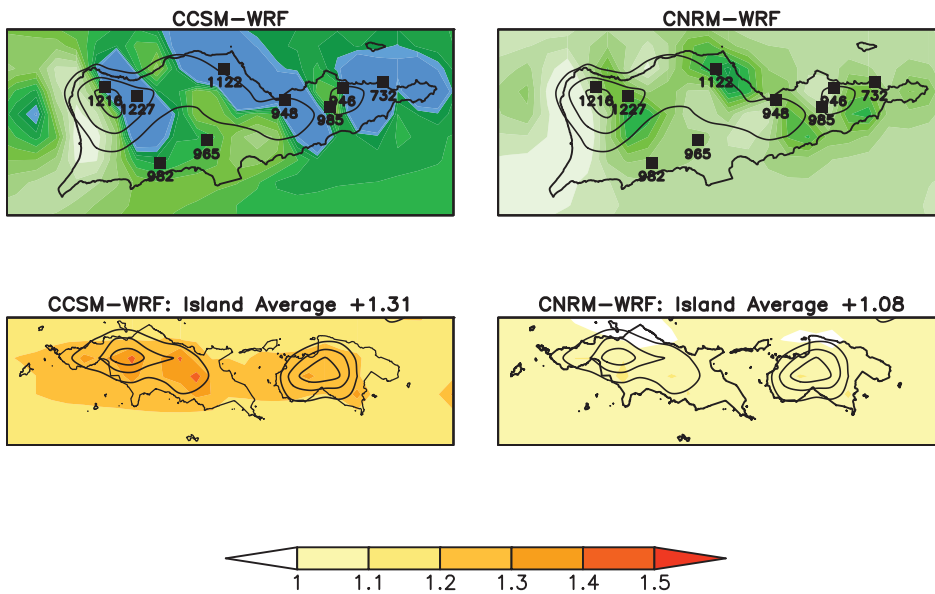
FIGURE 17 Projected change in annual average maximum temperature for St. Croix (top) and St. Thomas and St John (top) and St. Croix (bottom) from the WRF realizations for RCP8.5 at mid-century (2041-2060) for CCSM-WRF (left) and CNRM-WRF (right). Contours represent the model elevation starting with the first contour at 50 m (not labelled)

FIGURE 18 Percent change in the annual average precipitation for St. Croix (top) and St. Thomas and St John (bottom) from the WRF realizations for RCP8.5 at mid-century (2041-2060) for CCSM-WRF (left) and CNRM-WRF (right). Contours represent the model elevation starting with the first contour at 50 m (not labelled)

ACKNOWLEDGEMENTS

ORCID

Jared H. Bowden ⬭ https://orcid.org/0000-0002-1677-4292

Vasu Misra ⬭ https://orcid.org/0000-0002-1345-6280

Adrienne Wootten ⬭ https://orcid.org/0000-0001-6004-5823

REFERENCES

Álvarez-Berríos, N.L., Soto-Bayó, S., Holupchinski, E., Fain, S.J. and Gould, W.A. (2018) Correlating drought conservation practices and drought vulnerability in a tropical agricultural system. *Renewable Agriculture and Food Systems*, 33, 279–291. https://doi.org/10.1017/S174217051800011X.

Arguez, A., Durre, I., Applequist, S., Vose, R.S., Squires, M.F., Yin, X., Heim, R.R., Jr. and Owen, T.W. (2012) NOAA's 1981-2010 U.S. climate normals: an overview. *Bulletin of the American Meteorological Society*, 93, 1687–1697. https://doi.org/10.1175/BAMS-D-11-00197.1.

Allen, K., Dupuy, J.M., Gei, M.G., Hulshof, C., Medvigy, D., Pizano, C., Salgado-Negret, B., Smith, C.M., Trierweiler, A., van Bloem, S.J., Waring, B.G., Xu, X. and Powers, J.S. (2017) Will seasonally dry tropical forests be sensitive or resistant to future changes in rainfall regimes? *Environmental Research Letters*, 12, 023001. https://doi.org/10.1088/1748-9326/aa5968.

Beljaars, A.C.M. and Holtslag, A.A.M. (1991) Flux parameterization over land surfaces for atmospheric models. *Journal of Applied Meteorology*, 30, 327–341. http://doi.org/10.1175/1520-0450(1991)030%253C0327:FPOLSF%253E2.0.CO;2.

Bellenger, H., Guilyardi, E., Lelooup, J., Lengaigne, M. and Vialard, J. (2014) ENSO representation in climate models: from CMIP3 to CMIP5. *Climate Dynamics*, 42, 1999–2018. https://doi.org/10.1007/s00382-013-1783-z.

Bhardwaj, A., Misra, V., Mishra, A., Wootten, A., Boyles, R., Bowden, J.H. and Terando, A.J. (2018) Downscaling future climate projections over Puerto Rico using a non-hydrostatic atmospheric model. *Climatic Change*, 147, 133–147. https://doi.org/10.1007/s10584-017-2130-x.

Bowden, J.H., Otte, T.L., Nolte, C.G. and Otte, M.J. (2012) Examining interior grid nudging techniques using two-way nesting in the WRF model for regional climate modeling. *Journal of Climate*, 25, 2805–2823. https://doi.org/10.1175/JCLI-D-11-00167.1.

Bowden, J.H., Nolte, C.G. and Otte, T.L. (2013) Simulating the impact of the large-scale circulation on the 2-m temperature and precipitation climatology. *Climate Dynamics*, 40, 1903–1920. https://doi.org/10.1007/s00382-012-1440-y.

Brandeis, T., Helmer, E.H., Marcano-Vega, H. and Lugo, A.E. (2009) Climate shapes the novel plant communities that form after deforestation in Puerto Rico and the U.S. Virgin Islands. *Forest Ecology and Management*, 258, 1704–1718.

Campbell, J.D., Taylor, M.A., Stephenson, T.S., Watson, R.A. and Whyte, F.S. (2011) Future climate of the Caribbean from a regional climate model. *International Journal of Climatology*, 31, 1866–1878. https://doi.org/10.1002/joc.2200.

Chen, F. and Dudhia, J. (2001) Coupling an advanced land surface-hydrology model with the Penn State-NCAR MM5 modeling system. Part I: model implementation and sensitivity. *Monthly Weather Review*, 129, 569–585. https://doi.org/10.1175/1520-0493(2001)129%3C0569:CAALSH%3E2.0.CO;2.

Chou, M.D. and Lee, K.-T. (1996) Parameterizations for the absorption of solar radiation by water vapor and ozone. *Journal of the Atmospheric Sciences*, 53, 1203–1208. https://doi.org/10.1175/1520-0469(1996)053%3C1203:PFTAOS%3E2.0.CO;2.

Chou, M.D. and Suarez, M.J. (1994) An efficient thermal infrared radiation parameterization for use in general circulation models. *NASA Technical Memorandum*, 104606(3), 1–85.

Dai, A. (2013) Increasing drought under global warming in observations and models. *Nature Climate Change*, 3, 52–58.

Dai, A., Zhoa, T. and Chen, J. (2018) Climate change and drought: a precipitation and evaporation perspective. *Curr Clim Change Rep 4*, 301–312. https://doi.org/10.1007/s40641-018-0101-6.

Daly, C., Helmer, E.H. and Quinones, M. (2003) Mapping the climate of Puerto Rico, Vieques, and Culebra. *International Journal of Climatology*, 23, 1359–1381.

Deser, C., Knutti, R., Solomon, S. and Phillips, A.S. (2012) Communication of the role of natural variability in future North American climate. *Nature Climate Change*, 2, 775–779.

Dunne, J.P., John, J.G., Adcroft, A.J., Griffies, S.M., Hallberg, R. and Shevliakova, E. (2012) GFDL's ESM2 global coupled climate-carbon earth system models. Part I: physical formulation and baseline simulation characteristics. *Journal of Climate*, 25, 6646–6665. https://doi.org/10.1175/JCLI-D-11-00560.1.

Ek, M.B., Mitchell, K.E., Lin, Y., Rogers, E., Grunmann, P., Koren, V., Gayno, G. and Tarpley, J.D. (2003) Implementation of the Noah land surface model advances in the National Centers for environmental prediction operational mesoscale Eta model. *Journal of Geophysical Research-Atmospheres*, 108(D22), 8851. https://doi.org/10.1029/2002JD003296.

Emanuel, K. (2017) Will global warming make hurricane forecasting more difficult? *Bulletin of the American Meteorological Society*, 98, 495–501. https://doi.org/10.1175/BAMS-D-16-0134.1.

Ewel, J.J. and Whitmore, J.L. (1973) *The Ecological Life Zones of Puerto Rico and the US Virgin Islands, Research Paper ITF-18*. Rio Piedras: USDA Forest Service, Institute of Tropical Forestry. https://www.fs.usda.gov/treesearch/pubs/5551

Gent, P.R., Danabasoglu, G., Donner, L.J., Holland, M.M., Hunke, E.C., Jayne, S.R., Lawrence, D.M., Neale, R.B., Rasch, P.J., Vertenstein, M., Worley, P.H., Yang, Z.L. and Zhang, M. (2011) The community climate system model version 4. *Journal of Climate*, 24, 4973–4991. https://doi.org/10.1175/2011JCLI4083.1.

Hall, T.C., Sealy, A.M., Stephenson, T., Kusunoki, S., Taylor, M.A., Chen, A. and Kitoh, A. (2013) Future climate of the Caribbean from a super-high-resolution atmospheric general circulation model. *Theoretical and Applied Climatology*, 113, 271–287. https://doi.org/10.1007/s00704-012-0779-7.

Hayhoe, K. (2013) *Quantifying key drivers of climate variability and change for Puerto Rico and the Caribbean. Final report*. Agreement number G10AC00582, 1-241. http://www.pr-ccc.org/wp-content/uploads/2014/08/PP_1-52_Hayhoe_Caribbean_Final_Report.pdf

He, J. and Soden, B. (2017) A re-examination of the projected subtropical precipitation decline. *Nature Climate Change*, 7, 53–57. https://doi.org/10.1038/nclimate3157.

Held, I.M. and Soden, B.J. (2006) Robust responses of the hydrologic cycle to global warming. *Journal of Climate*, 19, 5686–5699. https://doi.org/10.1175/JCLI3990.1.

Henareh, A.K., Gould, W.A., Harmsen, E., Terando, A., Quinones, M. and Collazo, J.A. (2016) Climate change implications for tropical islands: interpolating and interpreting statistically downscaled GCM projections for management and planning. *Journal of Applied Meteorology and Climatology*, 55, 265–282. https://doi.org/10.1175/JAMC-D-15-0182.1.

Herwehe, J.A., Alapaty, K., Spero, T.L. and Nolte, C.G. (2014) Increasing the creditability of regional climate simulations by introducing subgrid-scale cloud radiation interactions. *Journal of Geophysical Research-Atmospheres*, 119, 5317–5330. https://doi.org/10.1002/2014JD021504.

Hong, S.-Y. and Pan, H.L. (1996) Nonlocal boundary layer vertical diffusion in a medium-range forecast model. *Monthly Weather Review*, 124, 2322–2339. https://doi.org/10.1175/1520-0493(1996)124%3C2322:NBLVDI%3E2.0.CO;2.

Hong, S.-Y. and Lim, J.-O.J. (2006) The WRF single moment 6-class microphysics scheme (WSM6). *Journal of the Korean Meteorological Society*, 42, 129–151.

Hong, S-Y, Noh, Y., and Dudhia, J. (2016) *A New Vertical Diffusion* Package with an Explicit Treatment of Entrainment Processes. Mon. Wea. Rev. 134(9), 2318-2341. https://doi.org/10.1175/MWR3199.1.

Iacono, M.J., Delamere, J.S., Mlawer, E.J., Shephard, M.W., Clough, S.A. and Collins, W.D. (2008) Radiative forcing by long-lived greenhouse gases: calculations with the AER radiative transfer models. *Journal of Geophysical Research*, 113, D13103. https://doi.org/10.1029/2008JD009944.

Ikawa, M. and Saito, K. (1991) Description of a non-hydrostatic model developed at the forecast research department of the MRI. *MRI Tech Report*, 28, 1–238. https://doi.org/10.11483/mritechrepo.28.

Jury, M.R. and Chiao, S. (2013) Leeside boundary layer confluence and afternoon thunderstorms over Mayaguez, Puerto Rico. *Monthly Weather Review*, 52, 439–454. https://doi.org/10.1175/JAMC-D-11-087.1.

Lau, K.M. and Kim, K.-M. (2015) Robust Hadley circulation changes and increasing global dryness due to CO_2 warming from CMIP5 model projections. *Proceedings of the National Academy of Sciences*, 112, 3630–3635. https://doi.org/10.1073/pnas.1418682112.

Lugo, A.E., Castro, L.M., Vale, A., López, T.M., Prieto, E.H., Martinó, A.G., Puente Rolón, A.R., Tossas, A.G., McFarlane, D.A., Miller, T., Rodríguez, A., Lundberg, J., Thomlinson, J., Colón, J., Schellekens, J.H., Ramos, O., and Helmer, E. (2001) Puerto Rican Karst-A Vital Resource. United States Department of Agriculture Forest Service Gen. Tech. Report WO-65. https://www.fs.usda.gov/treesearch/pubs/2864

Karmalkar, A.V., Taylor, M.A., Campbell, J., Stephenson, T., New, M., Centella, A., Benzanilla, A. and Charlery, J. (2013) A review of observed and projected changes in climate for islands in the Caribbean. *Atmosfera*, 26, 283–309. https://doi.org/10.1016/S0187-6236(13)71076-2.

Kanamitsu, M., Yoshimura, K., Yhang, Y.-B. and Hong, S.-Y. (2010) Errors of interannual variability and trend in dynamical downscaling of reanalysis. *Journal of Geophysical Research-Atmospheres*, 115, D17115. https://doi.org/10.1029/2009JD013511.

Knutson, T., Camargo, S.J., Chan, J.C.L., Emanuel, K., Ho, C.-H., Kossin, J., et al. (2019a) Tropical cyclones and climate change assessment: part I. Detection and Attribution. *Bulletin of the American Meteorological Society*, 100, 1987–2007. https://doi.org/10.1175/BAMS-D-18-0189.1.

Knutson, T., Camargo, S.J., Chan, J.C.L., Emanuel, K., Ho, C.-H., Kossin, J., Mohapatra, M., Satoh, M., Sugi, M., Walsh, K. and Wu, L. (2019b) Tropical cyclones and climate change assessment: part II. Projected response to anthropogenic warming. *Bulletin of the American Meteorological Society*, 101 E303–E322. https://doi.org/10.1175/BAMS-D-18-0194.1.

Knutti, R., Furrer, R., Tebaldi, C., Cermak, J. and Meehl, G.A. (2010) Challenges in combining projections from multiple climate models. *Journal of Climate*, 23, 2739–2758.

Kossin, J.P. and Vimont, D.J. (2007) A more general framework for understanding Atlantic hurricane variability and trends. *Bulletin of the American Meteorological Society*, 88, 1767–1781. https://doi.org/10.1175/BAMS-88-11-1767.

Kossin, J.P. (2017) Hurricane intensification along United States coast suppressed during active hurricane periods. *Nature*, 541, 390–393. https://doi.org/10.1038/nature20783.

Kossin, J.P. (2018) A global slowdown of tropical-cyclone translation speed. *Nature*, 558, 104–107. https://doi.org/10.1038/s41586-018-0158-3.

Mezghani, A., Dobler, A., Benestad, R., Haugen, J.E. and Pardking, K.M. (2019) Subsampling impact on the climate change signal over Poland based on simulations from statistical and dynamical downscaling. *Journal of Applied Meteorology and Climatology*, 58, 1061–1078.

Miller, G., and Lugo, A.E. (2009) *Guide to the ecological systems of Puerto Rico*. General Technical Report, IITF-GTR-35, 1-437 https://www.fs.usda.gov/treesearch/pubs/35382.

Misra, V. (2007) Addressing the issue of systematic errors in a regional climate model. *Journal of Climate*, 20, 801–818. https://doi.org/10.1175/JCLI4037.1.

Murphy, P.G., Lugo, A.E., Murphy, A.J. and Nepstad, D.C. (1995) The dry forests of Puerto Rico's south coast. In: Lugo, A.E. and Lowe, C. (Eds.) *Tropical Forests: Management and Ecology. Ecological Studies (Analysis and Synthesis)*, Vol. 112. New York, NY: Springer.

Nakanishi, M. and Niino, H. (2006) An improved Mellor-Yamada level-3 model: its numerical stability and application to a regional prediction of advection fog. *Boundary-Layer Meteorology*, 119, 397–407. https://doi.org/10.1007/s10546-005-9030-8.

Neelin, J.D., Münnich, M., Su, H., Meyerson, J.E. and Holloway, C. E. (2006) Tropical drying trends in global warming models and observations. *Proceedings of the National Academy of Sciences*, 103, 6110–6115. https://doi.org/10.1073/pnas.0601798103.

National Centers for Environmental Information (NOAA NCEI) (2019) *U.S. billion-dollar weather and climate disasters*. Available at: https://www.ncdc.noaa.gov/billions

Otte, T.L., Nolte, C.G., Otte, M.J. and Bowden, J.H. (2012) Does nudging squelch the extremes in regional climate modeling? *Journal of Climate*, 25, 7046–7066. https://doi.org/10.1175/JCLI-D-12-00048.1.

Pan, H. and Wu, W. (1995) Implementing a mass-flux convective parameterization package for the NHM medium range forecast model. *NHM Office Note* 409 https://repository.library.noaa.gov/view/noaa/11429.

Pasch, R., Penny, A.B. and Berg, R. (2019) National hurricane center tropical cyclone report. *Hurricane Maria (AL 152017)*.

Pfahl, S., O'Gorman, P.A. and Fischer, E.M. (2017) Understanding the regional pattern of projected future changes in extreme precipitation. *Nature Climate Change*, 7, 423–427. https://doi.org/10.1038/nclimate3287.

Rasmussen, R., Liu, C., Ikeda, K., Gochis, D., Yates, D., Chen, F., Tewari, M., Barlage, M., Dudhia, J., Yu, W. and Miller, K. (2011) High-resolution coupled climate runoff simulations of seasonal snowfall over Colorado: a process study of current and warmer climate. *Journal of Climate*, 24, 3015–3048. https://doi.org/10.1175/2010JCLI3985.1.

Riahi, K., Rao, S., Volker, K., Cho, C., Chirkov, V., Fischer, G., et al. (2011) RCP8.5 – a scenario of comparatively high greenhouse gas emissions. *Climatic Change*, 109, 33–57. https://doi.org/10.1007/s10584-011-0149-y.

Ryu, J.-H. and Hayhoe, K. (2014) Understanding the sources of Caribbean precipitation biases in CMIP3 and CMIP5 simulations. *Climate Dynamics*, 42, 3233–3252. https://doi.org/10.1007/s00382-013-1801-1.

Saito, K., Fujita, T., Yamada, Y., Ishida, J., Kumagai, Y., Aranami, K., et al. (2006) The operational JMA nonhydrostatic mesoscale model. *Monthly Weather Review*, 134, 1266–1298. https://doi.org/10.1175/MWR3120.1.

Santer, B.D., Taylor, K.E., Gleckler, P.J., Bonfils, C., Barnett, T.P., Pierce, D.W., Wigley, T.M.L., Mears, C., Wentz, F.J., Brüggemann, W., Gillett, N.P., Klein, S.A., Solomon, S., Stott, P.A., and Whener, M.F. (2009) Incorporating model quality information in climate change detection and attribution studies, PNAS, 106, 14778–14783. https://doi.org/10.1073/pnas.0901736106.

Santos-Burgoa, C., Goldman, A., Andrade, E., Barrett, N., Colon-Ramos, U., Edberg, M., Garcia-Meza, A., Goldman, L., Roess, A., Sandberg, J., and Zeger, S. (2018) *Ascertainment of the estimated excess mortality from Hurricane Maria in Puerto*. Available at: https://hsrc.himmelfarb.gwu.edu/sphhs_global_facpubs/288

Slingo, J.M. (1987) The development and verification of a cloud prediction scheme for the ECMWF model. *Quarterly Journal of the Royal Meteorological Society*, 113, 899–927. https://doi.org/10.1002/qj.49711347710.

Skamarock, W.C. and Klemp, J.B. (2008) A time-split non-hydrostatic atmospheric model for weather research and forecasting applications. *Journal of Computational Physics*, 227, 3465–3485. https://doi.org/10.1016/j.jcp.2007.01.037.

Sugi, M., Kuma, K., Tada, K., Tamiya, K. and Hasegawa, N. (1990) Description and performance of the JMA operational global spectral model (JMA-GSM88). *Geophysical Magazine*, 43, 105–130.

Taylor, K.E., Stouffer, R.J. and Meehl, G.A. (2012) An overview of CMIP5 and the experiment design. *Bulletin of the American Meteorological Society*, 93, 485–498. https://doi.org/10.1175/BAMS-D-11-00094.1.

Taylor, M.A. and Clarke, L.A. (2018) Future Caribbean climate in a world of rising temperatures. The 1.5 vs. 2.0 dilemma. *Journal of Climate*, 31, 2907–2926. https://doi.org/10.1175/JCLI-D-17-0074.1.

Tiedtke, M., Heckley, W.A. and Slingo, J. (1988) Tropical forecasting at ECMWF: the influence of physical parameterization on the mean structure of forecasts and analyses. *Quarterly Journal of the Royal Meteorological Society*, 114, 639–664. https://doi.org/10.1002/qj.49711448106.

Van Beusekom, A.E., González, G. and Rivera, M.M. (2016) Short-term precipitation and temperature trends along an elevation gradient in northeastern Puerto Rico. *Earth Interactions*, 19, 1–33. https://doi.org/10.1175/EI-D-14-0023.1.

Vimont, D.J. and Kossin, J.P. (2007) The Atlantic meridional mode and hurricane activity. *Geophysical Research Letters*, 34, L07709. https://doi.org/10.1029/2007GL029683.

Voldoire, A., Sanchez-Gomez, E., Salas y Mélia, D., Decharme, B., Cassou, C., Sénési, S., et al. (2013) The CNRM-CM5.1 global climate model: description and basic evaluation. *Climate Dynamics*, 40, 2091–2121. https://doi.org/10.1007/s00382-011-1259-y.

Wang, C., Lee, S.-K. and Enfield, D.B. (2008) Atlantic warm pool acting as a link between Atlantic multidecadal oscillation and Atlantic tropical cyclone activity. *Geochemistry, Geophysics, Geosystems*, 9, 1–17. https://doi.org/10.1029/2007GC001809.

Wilks, D.S. (2006) *Statistical Methods in the Atmospheric Sciences*. London: Academic Press. https://www.elsevier.com/books/statistical-methods-in-the-atmospheric-sciences/wilks/978-0-12-751966-1

Wootten, A., Bowden, J.H., Boyles, R. and Terando, A. (2016) The sensitivity of WRF downscaled precipitation in Puerto Rico to cumulus parameterization and interior grid nudging. *Journal of Applied Meteorology and Climatology*, 55, 2263–2281. https://doi.org/10.1175/JAMC-D-16-0121.

SUPPORTING INFORMATION

Additional supporting information may be found online in the Supporting Information section at the end of this article.